Clinical Science (2022) **136** 1661–1681
https://doi.org/10.1042/CS20220607

Research Article

Cardiomyocyte BRAF is a key signalling intermediate in cardiac hypertrophy in mice

Hajed O. Alharbi[1,*], Michelle A. Hardyman[1,*], Joshua J. Cull[1], Thomais Markou[1], Susanna T.E. Cooper[2], Peter E. Glennon[3], Stephen J. Fuller[1], Peter H. Sugden[1] and Angela Clerk[1]

[1]School of Biological Sciences, University of Reading, Reading, U.K.; [2]Molecular and Clinical Sciences Institute, St. George's University of London, London, U.K.; [3]University Hospitals Coventry and Warwickshire, University Hospital Cardiology Department, Clifford Bridge Road, Coventry, U.K.

Correspondence: Angela Clerk (a.clerk@reading.ac.uk)

Cardiac hypertrophy is necessary for the heart to accommodate an increase in workload. Physiological, compensated hypertrophy (e.g. with exercise) is reversible and largely due to cardiomyocyte hypertrophy. Pathological hypertrophy (e.g. with hypertension) is associated with additional features including increased fibrosis and can lead to heart failure. RAF kinases (ARAF/BRAF/RAF1) integrate signals into the extracellular signal-regulated kinase 1/2 cascade, a pathway implicated in cardiac hypertrophy, and activation of BRAF in cardiomyocytes promotes compensated hypertrophy. Here, we used mice with tamoxifen-inducible cardiomyocyte-specific BRAF knockout (CM-BRAFKO) to assess the role of BRAF in hypertension-associated cardiac hypertrophy induced by angiotensin II (AngII; 0.8 mg/kg/d, 7 d) and physiological hypertrophy induced by phenylephrine (40 mg/kg/d, 7 d). Cardiac dimensions/functions were measured by echocardiography with histological assessment of cellular changes. AngII promoted cardiomyocyte hypertrophy and increased fibrosis within the myocardium (interstitial) and around the arterioles (perivascular) in male mice; cardiomyocyte hypertrophy and interstitial (but not perivascular) fibrosis were inhibited in mice with CM-BRAFKO. Phenylephrine had a limited effect on fibrosis but promoted cardiomyocyte hypertrophy and increased contractility in male mice; cardiomyocyte hypertrophy was unaffected in mice with CM-BRAFKO, but the increase in contractility was suppressed and fibrosis increased. Phenylephrine induced a modest hypertrophic response in female mice and, in contrast with the males, tamoxifen-induced loss of cardiomyocyte BRAF reduced cardiomyocyte size, had no effect on fibrosis and increased contractility. The data identify BRAF as a key signalling intermediate in both physiological and pathological hypertrophy in male mice, and highlight the need for independent assessment of gene function in females.

Introduction

Cardiac hypertrophy is an important adaptive process required for the adult heart to accommodate an increase in workload. This may reflect 'normal' life processes such as exercise or pregnancy, in which case the adaptation is largely reversible and described as physiological [1]. It is also necessary to accommodate stresses such as hypertension and this pathological hypertrophy is generally not reversible. Although the initial hypertrophy compensates for the developing disease, this can degenerate over time resulting in decompensation and heart failure. The adult mammalian heart is comprised largely of terminally differentiated contractile cardiomyocytes with a network of capillaries that deliver blood throughout the heart from arterioles penetrating the myocardium. In addition, resident fibroblasts produce sufficient extracellular matrix for the heart to function. Irrespective of stimulus, the heart responds to an increased workload with hypertrophic growth of cardiomyocytes (in the absence of cell division) to increase contractile function [1]. In physiological hypertrophy (e.g. in response to exercise), this is beneficial and reversible, with little or no increase in fibrosis. In pathological conditions, cardiomyocyte hypertrophy

*These authors contributed equally to this work.

Received: 07 September 2022
Revised: 31 October 2022
Accepted: 03 November 2022

Accepted Manuscript online: 04 November 2022
Version of Record published: 21 November 2022

Clinical Science (2022) **136** 1661–1681
https://doi.org/10.1042/CS20220607

is compromised by other pathological changes. These include loss of the capillary network and increased myocardial fibrosis, both of which potentially lead to cardiomyocyte dysfunction and cell death with a reduction in contractile ability of the heart. Understanding the molecular basis of these changes will aid in identifying therapeutic approaches for the treatment of heart failure, the main goals being to sustain cardiomyocyte function and survival, maintain the capillary network and prevent cardiac fibrosis [2].

A key signalling pathway linked to cardiac hypertrophy is the extracellular signal-regulated kinase 1/2 (ERK1/2) cascade. Activation of ERK1/2, the 'original' mitogen-activated protein kinases (MAPKs), in cardiomyocytes promotes hypertrophic growth [3–5], but activation in cardiac fibroblasts promotes fibrosis [6,7]. *In vivo* studies in mice show that mild constitutive-activation of the pathway in cardiomyocytes promotes compensated hypertrophy, whilst cardiomyocyte-specific gene deletion experiments indicate that ERK1/2 are not just important for hypertrophic growth but are also cytoprotective [5,8–11]. ERK1/2 are phosphorylated and activated by MAPK kinases 1/2 (MKK1/2) which are, in turn, phosphorylated by one or more of the RAF kinases (RAF1, BRAF, ARAF) [12]. RAF kinases form an integrating node into the cascade and are intimately linked to cancer. Indeed, oncogenic mutations in BRAF cause up to 30% of all cancers, and small molecule inhibitors of RAF kinases are already in use as anti-cancer drugs [13]. However, RAF kinases are not equivalent and their regulation is complex involving spatial organization and interactions with multiple proteins, in addition to activating and inhibitory phosphorylations [12]. Importantly, although all RAF kinases can activate MKK1/2, ARAF and RAF1 have additional cytoprotective effects and inhibit pro-apoptotic kinases [14,15].

Despite their importance, there are still relatively few studies of RAF kinases in cardiomyocytes and the heart. BRAF expression is up-regulated in dilated cardiomyopathy and heart failure [16], suggesting it plays a role in human heart diseases. RAF1 and ARAF mRNAs are both down-regulated in dilated cardiomyopathy, although there may be differential regulation of RAF1 in some forms of heart failure. All RAF kinases are expressed in rodent cardiomyocytes and are activated by hypertrophic stimuli such as endothelin-1 or α_1-adrenergic receptor agonists [17,18]. *In vivo* studies in mice indicate that RAF1 is cytoprotective in cardiomyocytes, since overexpression of a dominant-negative form of RAF1 in cardiomyocytes or cardiomyocyte-specific RAF1 knockout leads to increased cardiomyocyte apoptosis and heart failure [19]. Activation of BRAF in cardiomyocytes by knock-in of the oncogenic V600E mutation promotes cardiomyocyte hypertrophy and compensated cardiac hypertrophy in mice [16] similar to that induced by overexpression of constitutively-active MKK1 [8]. Interestingly, RAF kinase inhibitors appear to have different effects on the heart. In a mouse model of hypertension induced by AngII, dabrafenib inhibits both cardiomyocyte hypertrophy and cardiac fibrosis [20]. In contrast, encorafenib activates ERK1/2 signalling (via the RAF paradox [12]) and promotes compensated cardiac hypertrophy in a similar manner to knock-in of the BRAF(V600E) mutation [16]. These studies demonstrate that BRAF is important in cardiomyocytes and has the potential to drive cardiac and cardiomyocyte hypertrophy, but do not establish any involvement in cardiac hypertrophy, whether physiological or pathological.

Here, we developed a mouse model for inducible cardiomyocyte-specific knockout of BRAF. We show that BRAF is required for cardiac adaptation to AngII, influencing both cardiomyocyte hypertrophy and fibrosis, but it plays a more subtle role affecting contractility and suppressing fibrosis in a model more akin to physiological hypertrophy. As with most studies, these experiments were conducted in male mice, but we also present data for physiological hypertrophy in female mice showing a different response to the males. These data highlight the need for full and proper experimental assessment of the underlying mechanisms of cardiac hypertrophy in females.

Methods

Ethics statement for animal experiments

Mice were housed at the BioResource Unit at University of Reading or the BioResource Facility at St. George's University of London (both U.K. registered with a Home Office certificate of designation). Experiments with AngII were conducted at University of Reading. Experiments with phenylephrine were conducted equally at University of Reading and St. George's University of London because experiments were interrupted at University of Reading due to the COVID-19 pandemic. Pilot studies at St. George's University of London confirmed that the responses were similar to those at University of Reading. All procedures were performed in accordance with U.K. regulations and the European Parliament Directive 2010/63/EU for animal experiments. Work was undertaken in accordance with local institutional animal care committee procedures at both institutions and the U.K. Animals (Scientific Procedures) Act 1986. Studies were conducted under Project Licences 70/8249 (University of Reading) and P8BAB0744 (both institutions).

In vivo studies of mice with cardiomyocyte-specific deletion of BRAF

Housing conditions were as described in [16,21]. Breeding was conducted with mice between 6 weeks and 8 months with a maximum of 4 litters per female. Mice undergoing procedures were monitored using a score sheet and routinely culled if they reached a predefined endpoint agreed with the Named Veterinary Surgeon. Weights were taken before, during and at the end of the procedures. Mouse weights from the start and end of procedures are provided in Supplementary Table S1. Mice were allocated to specific groups on a random basis with randomization performed independently of the individual leading the experiment. No mice were excluded after randomization. Individuals conducting the studies were not blinded to experimental conditions for welfare monitoring purposes. Data and sample analysis (e.g. echocardiography, histology) were performed by individuals who were blinded to intervention.

Mouse lines

Genetically modified mice were from Jackson Laboratories, imported into the U.K. and transported to University of Reading for breeding in-house. We used mice with a floxed cassette for Cre-induced BRAF gene deletion (129-*Braf*^{tm1Sva}/J, strain no. 006373) [22]. Mice were backcrossed against the C57Bl/6J background at University of Reading for at least 4 generations prior to experimentation. Mice were bred with *Myh6*-MERCreMER mice expressing tamoxifen-inducible Cre recombinase under control of a mouse *Myh6* promoter [Tg(Myh6-cre)1Jmk/J, strain no. 009074] [23]. Breeding protocols were used to produce male and female BRAF$^{fl/fl}$/Cre$^{+/-}$ mice (i.e. homozygous for floxed BRAF and hemizygous for Cre) for experimentation. Mice hemizygous for Cre (Cre$^{+/-}$) were also generated from the same breeding stocks. Additional studies were conducted in parallel with wild-type mice from the same breeding stocks.

Genotyping and confirmation of recombination

DNA was extracted from ear clips (taken for identification purposes) using Purelink genomic DNA (gDNA) mini-kits (Invitrogen). Briefly, tissue was digested in genomic digestion buffer containing proteinase K (overnight, 55°C). Following centrifugation (12,000 × ***g***, 3 min, 18°C), supernatants were incubated with RNAse A (2 min) before addition of genomic lysis binding buffer mixed with an equal volume of ethanol. gDNA was purified using Purelink spin columns and PCR amplified with specific primers (see Supplementary Table S2 for primer sequences and annealing temperatures) using GoTaq Hot Start Polymerase (Promega). PCR conditions were 95°C for 3 min, followed by up to 33 cycles of 95°C denaturation for 30 s, 30 s annealing, elongation at 72°C for 30 s, followed by a 7 min 72°C final extension. PCR products were separated on 2% (w/v) agarose gels (25 min, 80 V) containing Sybr Green and visualized under UV light. Mice (males: 7–8 weeks; females: 9–10 weeks) were treated with a single dose of tamoxifen (40 mg/kg i.p.; Sigma-Aldrich) or vehicle alone. Tamoxifen was dissolved in 0.25 ml ethanol and then mixed with 4.75 ml corn oil. For confirmation of recombination, RNA was extracted from tissue powders and cDNA prepared as described below. cDNA (4 µl) was subjected to PCR analysis using GoTaq Hot Start Polymerase with specific primers and conditions (see Supplementary Table S2 for primer sequences and annealing temperatures). PCR conditions were 95°C for 3 min, followed by 32 cycles of 95°C denaturation for 30 s, 30 s at 57°C, elongation at 72°C for 60 s, followed by a 7 min 72°C final extension. Products were separated by electrophoresis on a 2% (w/v) agarose gel (85 V, 45 min).

Drug delivery to induce cardiac hypertrophy

Drug delivery used Alzet osmotic pumps (model 1007D; supplied by Charles River), filled according to the manufacturer's instructions in a laminar flow hood using sterile technique. Mice were treated with 0.8 mg/kg/d AngII in acidified PBS (PBS containing 10 mM acetic acid) or with acidified PBS alone as in [20,24]. We used 0.8 mg/kg/d AngII as a moderate concentration that gradually induces hypertension over 7–14 days [25–27] rather than a subpressor dose (e.g. 0.288 mg/kg/d [28]) or a high dose that can be associated with sudden cardiac death (e.g. >2 mg/kg/d [7]). Alternatively, mice were treated with 40 mg/kg/d phenylephrine in PBS or with PBS alone as in [29]. This is a relatively high dose that may increase blood pressure but the increase over 7 d is likely to be <10% as in [30]. Minipumps were incubated overnight in sterile PBS (37°C). Mice were given 0.05 mg/kg (s.c.) buprenorphine (Vetergesic, Ceva Animal Health Ltd.) before being placed under continuous inhalation anaesthesia using isoflurane (induction at 5%, maintenance at 2–2.5%) mixed with 2 l/min O_2. A 1 cm incision was made in the mid-scapular region and minipumps were implanted portal first in a pocket created in the left flank region of the mouse. Wound closure used wound clips or a simple interrupted suture with polypropylene 4-0 thread (Prolene, Ethicon). Mice were recovered singly and returned to their home cage once fully recovered.

Clinical Science (2022) **136** 1661–1681
https://doi.org/10.1042/CS20220607

Cardiac ultrasound

Echocardiography was performed using a Vevo 2100 equipped with a MS400 18-38 MHz transducer (Visualsonics) as in [16,20,29]. Mice were anaesthetized in an induction chamber with isoflurane (5% flow rate) with 1 l/min O_2 and transferred to the heated Vevo Imaging Station. Anaesthesia was maintained with 1.5% isoflurane delivered via a nose cone. Left ventricular cardiac function and structure was assessed from short axis M-mode images with the axis placed at the mid-level of the left ventricle at the level of the papillary muscles. Left ventricular mass and chamber volumes were measured from B-mode long axis images using VevoStrain software for speckle tracking. Baseline scans were taken prior to experimentation (7 to 3 days). Further scans were taken at intervals following minipump implantation. Imaging was completed within 20 min. Data analysis (Vevo LAB) was performed by an independent assessor blinded to intervention. Data were gathered from two scans taken from each time point, taking mean values across four cardiac cycles for each M-mode scan or two cardiac cycles for long axis B-mode images. Mice were recovered singly and transferred to the home cage once fully recovered.

Tissue harvesting and histology

Mice were culled by CO_2 inhalation followed by cervical dislocation. Hearts were excised quickly, washed in PBS, dried and snap-frozen in liquid N_2 or fixed for histology. Histological sections were prepared and stained by HistologiX Limited. Haemotoxylin and eosin staining was used for analysis of myocyte cross-sectional area. Cells around the periphery of the left ventricle (excluding epicardial layer) were chosen at random and outline traced using NDP.view2 software (Hamamatsu). Up to 30 cells were measured per section by a single independent assessor and the mean value taken for each mouse. To assess fibrosis to show the relative amount in wild-type compared with $BRAF^{fl/fl}/Cre^{+/-}$ mice, sections were stained with Masson's trichrome and analysis used Image-J as in [24]. The collagen fraction was calculated as the ratio between the sum of the total area of fibrosis (blue colour) to the sum of the total tissue area (including the myocyte area) for the entire image and expressed as a percentage. For other studies, the amount of fibrosis was determined using picrosirius red staining and the whole section was scored for perivascular fibrosis around arterioles (identified by a clear elastic layer) and interstitial fibrosis. For perivascular fibrosis values were from 1 (negligible increase in fibrosis around any vessel) to 4 (extensive fibrosis around multiple vessels, penetrating into the myocardium). For interstitial fibrosis values were from 1 (negligible increase in fibrosis within the myocardium distal from any arterioles) to 4 (extensive and pervasive fibrosis throughout the left ventricle).

RNA preparation and qPCR

Mouse heart powders were weighed into safelock Eppendorf tubes and kept on dry ice. RNA Bee (AMS Biotechnology Ltd) was added (1 ml per 10–15 mg) and the samples homogenized on ice using a pestle. RNA was prepared according to the manufacturer's instructions and dissolved in nuclease-free water. The purity was assessed from the A_{260}/A_{280} measured using an Implen NanoPhotometer (values were 1.8–2.0) and concentrations determined from the A_{260}. Quantitative PCR (qPCR) analysis was performed as described in [31]. Total RNA (1 μg) was reverse transcribed to cDNA using High Capacity cDNA Reverse Transcription Kits with random primers (Applied Biosystems). qPCR was performed using an ABI Real-Time PCR 7500 system (Applied Biosystems) using 1/40 of the cDNA produced. Optical 96-well reaction plates were used with iTaq Universal SYBR Green Supermix (Bio-Rad Laboratories Inc.) according to the manufacturer's instructions. See Supplementary Table S3 for primer sequences. Results were normalized to *Gapdh*, and relative quantification was obtained using the ΔCt (threshold cycle) method; relative expression was calculated as $2^{-\Delta\Delta Ct}$, and normalized as indicated in the figure legends.

Immunoblotting

Heart powders (15–20 mg) were extracted in 6 vol extraction buffer [20 mM Tris pH 7.5, 1 mM EDTA, 10% (v/v) glycerol, 1% (v/v) Triton X-100, 100 mM KCl, 5 mM NaF, 0.2 mM Na_3VO_4, 5 mM $MgCl_2$, 0.05% (v/v) 2-mercaptoethanol, 10 mM benzamidine, 0.2 mM leupeptin, 0.01 mM trans-epoxy succinyl-l-leucylamido-(4-guanidino)butane, 0.3 mM phenylmethylsulphonyl fluoride, 4 μM microcystin]. Samples were vortexed and extracted on ice (10 min), then centrifuged (10,000 × ***g***, 10 min, 4°C). The supernatants were removed, a sample was taken for protein assay and the rest boiled with 0.33 vol sample buffer (300 mM Tris-HCl pH 6.8, 10% (w/v) SDS, 13% (v/v) glycerol, 130 mM dithiothreitol, 0.2% (w/v) bromophenol blue). Protein concentrations were determined by BioRad Bradford assay using BSA standards.

Proteins were separated by SDS-PAGE (200 V) using 8% (for RAF kinases), or 12% (Gapdh) polyacrylamide resolving gels with 6% stacking gels until the dye front reached the bottom of the gel (∼50 min). Proteins were transferred electrophoretically to nitrocellulose using a BioRad semi-dry transfer cell (10 V, 60 min). Non-specific binding sites were blocked (15 min) with 5% (w/v) non-fat milk powder in Tris-buffered saline (20 mM Tris-HCl pH 7.5, 137

mM NaCl) containing 0.1% (v/v) Tween 20 (TBST). Blots were incubated with primary antibodies in TBST containing 5% (w/v) BSA (overnight, 4°C), then washed with TBST (3 × 5 min, 21°C), incubated with horseradish peroxidase-conjugated secondary antibodies in TBST containing 1% (w/v) non-fat milk powder (60 min, 21°C) and then washed again in TBST (3 × 5 min, 21°C). Antibodies to RAF1 were from BD Transduction Labs (mouse monoclonal, Cat. No. 610152), antibodies to BRAF and ARAF were from Santa Cruz Biotechnology Inc. (BRAF: mouse monoclonal, Cat. No. sc-5284; ARAF: rabbit polyclonal, Cat. No. sc-408), antibodies to Gapdh (rabbit monoclonal, Cat. No. 5174), phosphorylated ERK1/2(T202/Y204) (rabbit monoclonal, Cat. No. 4377) and total ERK1/2 (rabbit monoclonal, Cat. No. 4695) were from Cell Signaling Technologies and secondary antibodies were from Dako, supplied by Agilent (rabbit anti-mouse immunoglobulins/HRP, Cat. No. P0260; goat anti-rabbit immunoglobulins/HRP, Cat. No. P0448). Primary antibodies were used at 1/1000 dilution. Secondary antibodies were used at 1/5000 dilution.

Bands were detected by enhanced chemiluminescence using ECL Prime with visualization using an ImageQuant LAS4000 system (Cytiva). ImageQuant TL 8.1 software (GE Healthcare) was used for densitometric analysis. Raw values for phosphorylated kinases were normalized to the total kinase. Values for all samples were normalized to the mean of the controls.

Image processing and statistical analysis

Images were exported from the original software as .tif or .jpg files and cropped for presentation using Adobe Photoshop CC maintaining the original relative proportions. Data analysis used Microsoft Excel and GraphPad Prism 9. Statistical analysis was performed using GraphPad Prism 9 with two-tailed unpaired *t* tests, or two-tailed one-way or two-way ANOVA as indicated in the Figure Legends. A Holm-Sidak's multiple comparison test was used in combination with ANOVA. A Grubb's outlier test was applied to the data, and outliers excluded from the analysis. Graphs were plotted with GraphPad Prism 9. Specific *P* values are provided with significance levels of $P<0.05$ in bold type.

Results

Cardiomyocyte BRAF knockout model

Our previous studies demonstrated that activation of BRAF in cardiomyocytes can promote hypertrophy [16], but this does not establish the role it may play in adaptation of the heart to pathophysiological stresses. To assess this, we generated mice for cardiomyocyte-specific inducible BRAF knockout by crossing mice with a floxed cassette for Cre-induced BRAF gene deletion [22] with *Myh6*-MERCreMER mice expressing tamoxifen-inducible Cre recombinase under control of a mouse *Myh6* promoter [23]. Experiments first used male mice homozygous for floxed BRAF and hemizygous for Cre ($BRAF^{fl/fl}/Cre^{+/-}$ mice). Baseline echocardiograms were collected at age 7–8 weeks, then cardiomyocyte BRAF knockout was induced by a single injection of tamoxifen (40 mg/kg i.p.). This dosage regime has the advantage that the tamoxifen is cleared from the body within 24–72 h [32] and induces recombination in the absence of significant cardiomyopathy [33]. We confirmed this previously in control experiments comparing tamoxifen treatment with vehicle controls in mice that were hemizygous for Cre ($Cre^{+/-}$) [16]. Additional control experiments conducted with $Cre^{+/-}$ mice derived from the $BRAF^{fl/fl}$ background also showed no significant effect of the tamoxifen/Cre combination on cardiac function or dimensions in the absence or presence of AngII (Supplementary Table S4). Recombination was confirmed at the mRNA level in different groups of mice (Figure 1A). Decreased expression of BRAF in the heart (0.66 ± 0.11 relative to mice treated with corn-oil) was confirmed by immunoblotting (Figure 1B). RAF1 (not ARAF) expression was also decreased (0.77 ± 0.13 relative to mice treated with corn-oil). This may be because BRAF forms heterodimers with RAF1 in cardiomyocytes [16], so loss of BRAF potentially affects expression of the pool of RAF1 with which it associates. Although cardiomyocytes constitute ∼70% of the volume of the heart, at most they represent ∼30% of the total cell number with cardiac non-myocytes (including fibroblasts and endothelial cells) accounting for the remainder [34]. In rodents, up to 90% of cardiomyocytes may be binucleated [35], so the maximum degree of down-regulation of BRAF that we might expect in the heart of a cardiomyocyte-specific knockout model is ∼45%. Our data indicate that, on average, we obtained ∼77% of this maximum value.

Tamoxifen and cardiomyocyte BRAF knockout alone had no significant effects on any of the parameters studied relative to $BRAF^{fl/fl}/Cre^{+/-}$ male mice treated with corn-oil vehicle (e.g. hypertrophic gene markers, Figure 1C) indicating that BRAF is not essential in normal adult mouse hearts, at least in the short term. Heart weight:body weight (HW:BW) ratios were similar in mice treated with/without tamoxifen (Supplementary Figure S1A), and $BRAF^{fl/fl}/Cre^{+/-}$ mice exhibited no baseline differences in heart morphology compared with wild-type C57Bl/6J mice from the same breeding stocks studied in parallel. At baseline, cardiomyocytes were of similar size and the

Clinical Science (2022) **136** 1661–1681
https://doi.org/10.1042/CS20220607

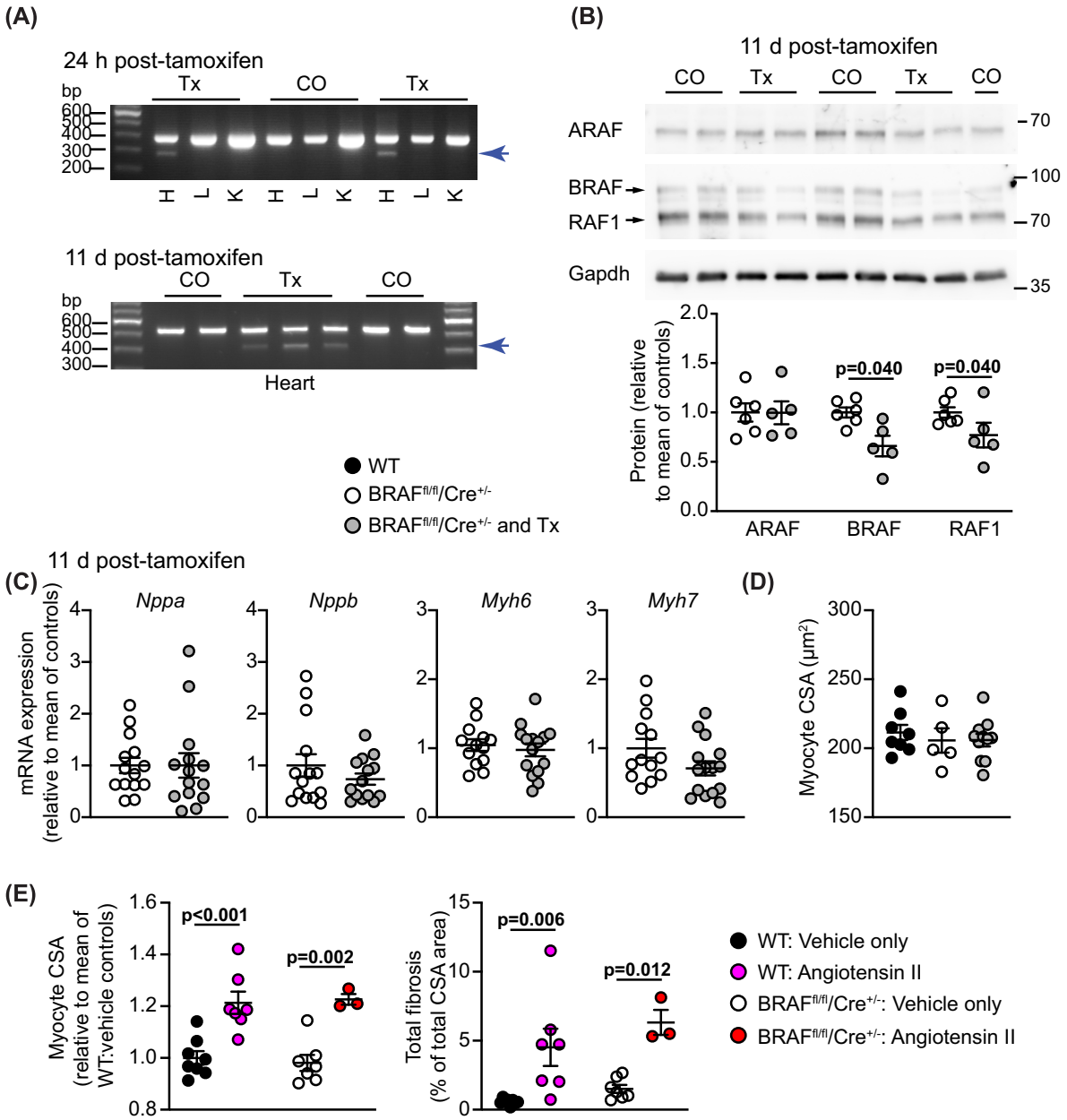

Figure 1. Male mice with tamoxifen-inducible cardiomyocyte-specific BRAF knockout

BRAF$^{fl/fl}$/Cre$^{+/-}$ (homozygous for floxed BRAF; hemizygous for Cre) male mice were treated with corn-oil (CO) or tamoxifen in CO (Tx) for 24 h or 11 d as indicated. (**A**) Confirmation of BRAF knockout using cDNA prepared from RNA extracted from powdered tissues. PCR amplification used forward primers in exon 10 (upper image) or exon 9 (lower image) with reverse primers in exon 13. Deletion of exon 12 in cardiomyocytes resulted in the appearance of a smaller product following recombination with tamoxifen administration in heart (H), but not liver (L) or kidney (K). Representative images are shown. (**B**) Immunoblot analysis of RAF isoforms in samples of mouse hearts treated with vehicle or tamoxifen. Representative immunoblots are in the upper panels (positions of relative molecular mass markers are on the right) with densitometric analysis below. RAF expression was normalized to Gapdh and data presented relative to the means of the vehicle treated controls. Statistical analysis used unpaired two-tailed *t* tests. (**C**) mRNA expression in mouse hearts after 11 d treatment with tamoxifen. RNA was extracted and expression of selected genes assessed by qPCR. (**D,E**) Assessment of cardiomyocyte cross-sectional area (CSA) and fibrosis in wild-type (WT) mice from the same breeding stock as the BRAF$^{fl/fl}$/Cre$^{+/-}$ mice in comparison with the BRAF$^{fl/fl}$/Cre$^{+/-}$ mice. Mice were treated with Tx for 11 d, AngII (0.8 mg/kg/d, 7 d) in acidified PBS (AcPBS) or AcPBS only. Data for CSA are from haematoxylin and eosin stained sections. Data for fibrosis are from Masson's trichrome and picrosirius red stained sections. Data are presented as individual values with means ± SEM. Statistical analysis used unpaired two-tailed *t* tests.

hypertrophic response in $BRAF^{fl/fl}/Cre^{+/-}$ mice induced by AngII (increase in cardiomyocyte size and left ventricular fibrosis) was also similar to wild-type mice (Figure 1D,E). In summary, we detected no significant baseline effects of the mutant genetic background in male mice with or without cardiomyocyte BRAF knockout.

Cardiomyocyte BRAF is required for cardiac adaptation to hypertension induced by AngII

We assessed the effects of BRAF knockout in a model of hypertension induced by treatment with 0.8 mg/kg/d AngII over 7 d (Figure 2A). This dose of AngII not only causes pressure-overload on the heart by increasing systemic blood pressure over 7–14 days [26,27] but also stimulates endothelial cells lining the blood vessels, acting directly on AngII receptors. Thus, the primary impact on the heart is first on the arteries/arterioles and, subsequently, on the rest of the myocardium. AngII in acidified PBS (AcPBS) or AcPBS alone was delivered by osmotic minipumps, implanted 4 d after tamoxifen administration, by which time tamoxifen has cleared the body [32]. At this early stage, AngII induced only a small increase in HW:BW ratio that was similar with and without tamoxifen treatment (Supplementary Figure S1A). However, as in previous studies [20,24], AngII promoted cardiac hypertrophy as assessed by echocardiography: left ventricular (LV) internal diameter and predicted end diastolic volume decreased, whilst LV wall thickness and predicted end diastolic LV mass were increased (Figure 2B,C and Supplementary Table S5). At 7 d, we detected no significant change in ejection fraction or fractional shortening (Supplementary Table S5). Cardiomyocyte-specific deletion of BRAF did not affect the decrease in LV internal diameter or volume but reduced AngII-induced increases in LV wall thickness and predicted mass (Figure 2B,C). AngII increased cardiomyocyte cross-sectional area (a measure of hypertrophy) to a similar degree in wild-type and $BRAF^{fl/fl}/Cre^{+/-}$ mice, and this was inhibited by cardiomyocyte BRAF knockout (Figures 1E and 2D).

Pathological hypertrophy is associated with increases in cardiac mRNA expression of the 'foetal' gene markers, *Nppa*, *Nppb*, and *Myh7*. These markers were not significantly changed with cardiomyocyte BRAF knockout alone, but AngII-induced increases in expression of *Nppa* and *Nppb* (not *Myh7*) were inhibited in mouse hearts with cardiomyocyte deletion of BRAF at 24 h (Figure 2E). By 7 d, the level of expression induced by AngII had declined and the effect of cardiomyocyte BRAF knockout on the *Nppa* and *Nppb* response was lost (Figure 2F). Cardiomyocyte hypertrophy may be stimulated by biomechanical stresses detected by mechanosensors in the cell (e.g. stretch-regulated ion channels [36] or the myofibrillar apparatus and other structural components [37]) that trigger changes in gene expression and cause hypertrophy. Additionally, neurohumoral mediators produced by the vessels may contribute. For example, endothelin-1 produced by endothelial cells in response to AngII [38] is a potent stimulus of cardiomyocyte hypertrophy, signalling through the ERK1/2 pathway [3]. Notably, endothelin-1 mRNA (*Edn1*) was up-regulated by AngII, a response that was unaffected by cardiomyocyte BRAF knockout (Figure 2F). Irrespective of the origin of the signal, cardiomyocyte BRAF is a key mediator of cardiomyocyte hypertrophy induced by AngII.

Cardiac hypertrophy is associated with cardiomyocyte growth but can also reflect increased fibrosis. This may be mediated via ERK1/2 signalling and influenced by cardiomyocytes acting on neighbouring cells (e.g. via paracrine mediators) [39–41]. AngII increased cardiac fibrosis (shown with picrosirius red staining), with a striking effect in the immediate environment of the arterioles within the myocardium (the 'perivascular' region; Figure 3A–C). AngII promoted a relatively small increase in interstitial fibrosis and this was generally in localized areas of the heart. Interstitial fibrosis, but not perivascular fibrosis, was reduced in hearts with cardiomyocyte BRAF knockout (Figure 3C). Thus, interstitial and perivascular fibrosis have independent origins and, whilst cardiomyocyte hypertrophy contributes to the accumulation of interstitial fibrosis, the impact of hypertension on the fibrosis surrounding arterioles is largely independent of cardiomyocyte involvement. The data are consistent with our observation that up-regulation of *Edn1* mRNA was not inhibited by cardiomyocyte BRAF knockout (Figure 2F) since mediators deriving from the vessels would not be expected to be affected. In contrast, accumulation of fibrotic material within the myocardium is potentially driven by the cardiomyocytes themselves. In support of this, *Fgf2* mRNA expression was significantly up-regulated in hearts of mice treated with AngII, and the increase in expression was reduced in mouse hearts with cardiomyocyte BRAF knockout (Figure 4A). In addition, mRNA expression of the pro-fibrotic factor, connective tissue growth factor (*Ctgf*) was significantly up-regulated within 1 d of angiotensin infusion (with an indication of increased expression at 7 d) and this was significantly inhibited by cardiomyocyte BRAF knockout (Figure 4B). mRNA expression of the associated pro-fibrotic factor, *Tgfb1*, responded similarly although the increase in expression was not statistically significant. The data are generally consistent with the concept of cross-talk between cardiomyocytes and the non-myocytes in the heart [42].

To gain further insight into the consequences of cardiomyocyte BRAF knockout for the heart in AngII-induced cardiac hypertrophy, we assessed mRNA expression of selected genes. Despite the effect on *Fgf2* (Figure 4A),

Clinical Science (2022) **136** 1661–1681
https://doi.org/10.1042/CS20220607

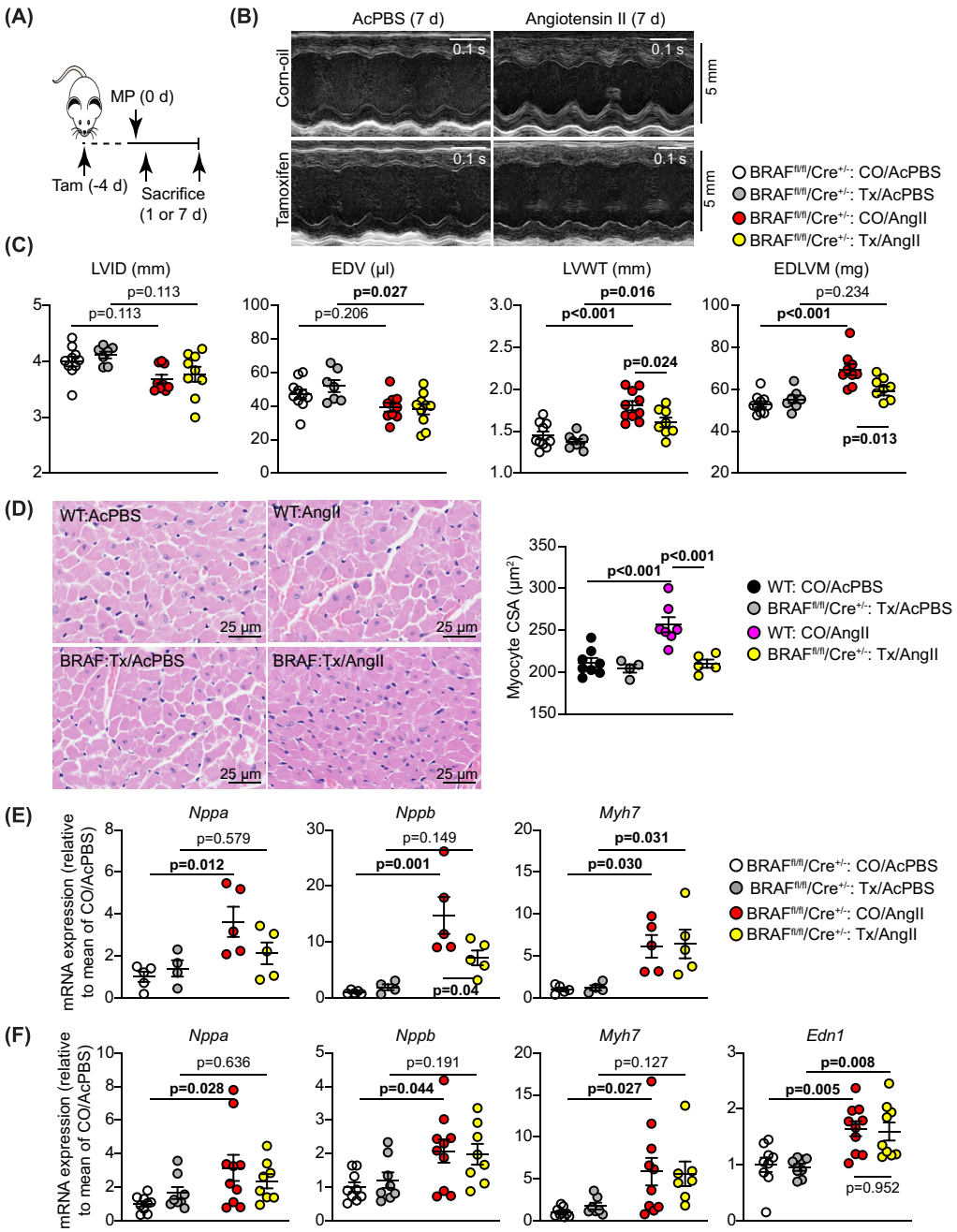

Figure 2. Cardiomyocyte BRAF knockout inhibits the hypertrophic response induced by AngII in male mouse hearts

Male BRAF$^{fl/fl}$/Cre$^{+/-}$ (BRAF) or wild-type (WT) mice were treated with corn-oil vehicle (CO) or tamoxifen in CO (Tx) 4 days before minipumps (MP) were implanted to deliver acidified PBS (AcPBS) or 0.8 mg/kg/d AngII. Mice were sacrificed after 1 or 7 d. Echocardiograms were collected and hearts taken at 7 d. (**A**) Schematic of experimental protocol. (**B**) Representative M-mode echocardiograms taken from short axis views of the hearts of BRAF$^{fl/fl}$/Cre$^{+/-}$ at 7 d. (**C**) Analysis of echocardiograms taken at 7 d to assess cardiac dimensions. Abbreviations: EDV, end diastolic volume; EDLVM, end diastolic left ventricular mass; LVID, left ventricle internal diameter; LVWT, left ventricle wall thickness (posterior plus anterior walls). LVID and LVWT were measured at diastole from M-mode images of short axis views of the heart. EDV and EDLVM were predicted from B-mode images of long axis views of the heart. (**D**) Haematoxylin and eosin staining of mouse heart sections (left panels) from hearts collected at 7 d, with assessment of cardiomyocyte cross-sectional area (CSA; right panel). Images and measurements are from the periphery of the left ventricle. (**E,F**) mRNA expression in mouse hearts after 24 h (E) or 7 d (F) treatment with AngII. RNA was extracted and expression of *Nppa*, *Nppb*, *Myh7* and *Edn1* were assessed by qPCR. Data are individual values with means ± SEM. Statistical analysis used two-way ANOVA with Holm-Sidak's post-test. Statistically significant values ($P<0.05$) are in bold type.

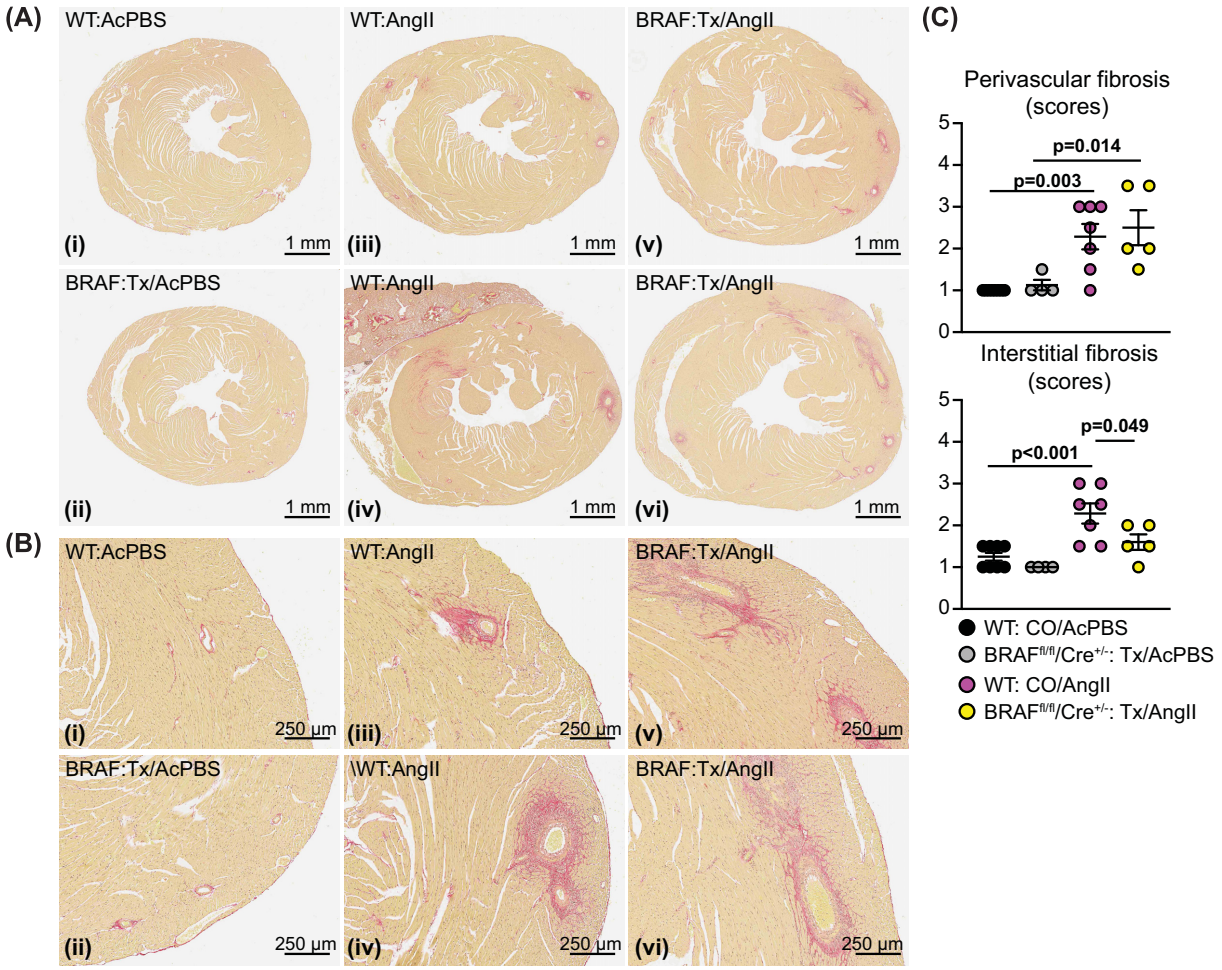

Figure 3. Cardiomyocyte BRAF knockout inhibits interstitial but not perivascular fibrosis induced by AngII in male mouse hearts

Male BRAF$^{fl/fl}$/Cre$^{+/-}$ (BRAF) or wild-type (WT) mice were treated with CO or tamoxifen in CO (Tx) 4 days before minipumps were implanted to deliver acidified PBS (AcPBS) or 0.8 mg/kg/d AngII in AcPBS (AngII) for 7 d. (**A,B**) Picrosirius red staining of mouse heart sections showing short axis views of the whole heart (A) with enlarged sections (B) from the same views (the red stain shows accumulation of fibrotic material). Representative (average) images are shown for mice treated with CO/AcPBS (i), Tx/AcPBS (ii), CO/AngII (iii) and Tx/AngII (v). Additional images are shown for the most severe degree of fibrosis with CO/AngII (iv) and Tx/AngII (vi). (**C**) Quantification of the degree of fibrosis. This was scored as: 1 = the least amount of fibrosis; 2 = low level fibrosis; 3 = high level fibrosis in at least one area of the myocardium; 4 = high level fibrosis throughout the myocardium (half scores were used). Statistical analysis used two-way ANOVA with Holm-Sidak's post-test. Statistically significant values ($P<0.05$) are in bold type.

up-regulation of fibrotic gene markers by AngII was generally enhanced in hearts from mice with cardiomyocyte BRAF knockout (Figure 4C), including the fibroblast marker *Ddr2*, collagens (*Col1a1*, *Col1a2*), other extracellular matrix proteins (*Postn*, *Fn1*) and lysyl oxidase (*Lox*) involved in collagen cross linking. This presumably reflects the prevalent fibrosis in the perivascular region (Figure 3A–C). Other genes associated with hypoxia (*Hif1a*) and inflammation (*IL1b*, *IL6*) were also enhanced in cardiomyocyte BRAF knockout hearts (Figure 4D) and may contribute to further development of fibrosis [39]. AngII-induced hypertrophy is associated with increased reactive oxygen species (ROS), potentially from NADPH oxidases NOX2 and NOX4 [43]. Consistent with other studies, NOX2 and NOX4 mRNA expression was increased with AngII (though not NOX1). As a constitutively active enzyme, NOX4 is predicted to increase cardiac oxidative stress [39,43]. Overall, these changes in gene expression indicate that the pathophysiological stresses resulting from AngII-induced hypertension were not ameliorated in the hearts with cardiomyocyte BRAF knockout and reduced cardiomyocyte hypertrophy and were, if anything, exacerbated.

Clinical Science (2022) **136** 1661–1681
https://doi.org/10.1042/CS20220607

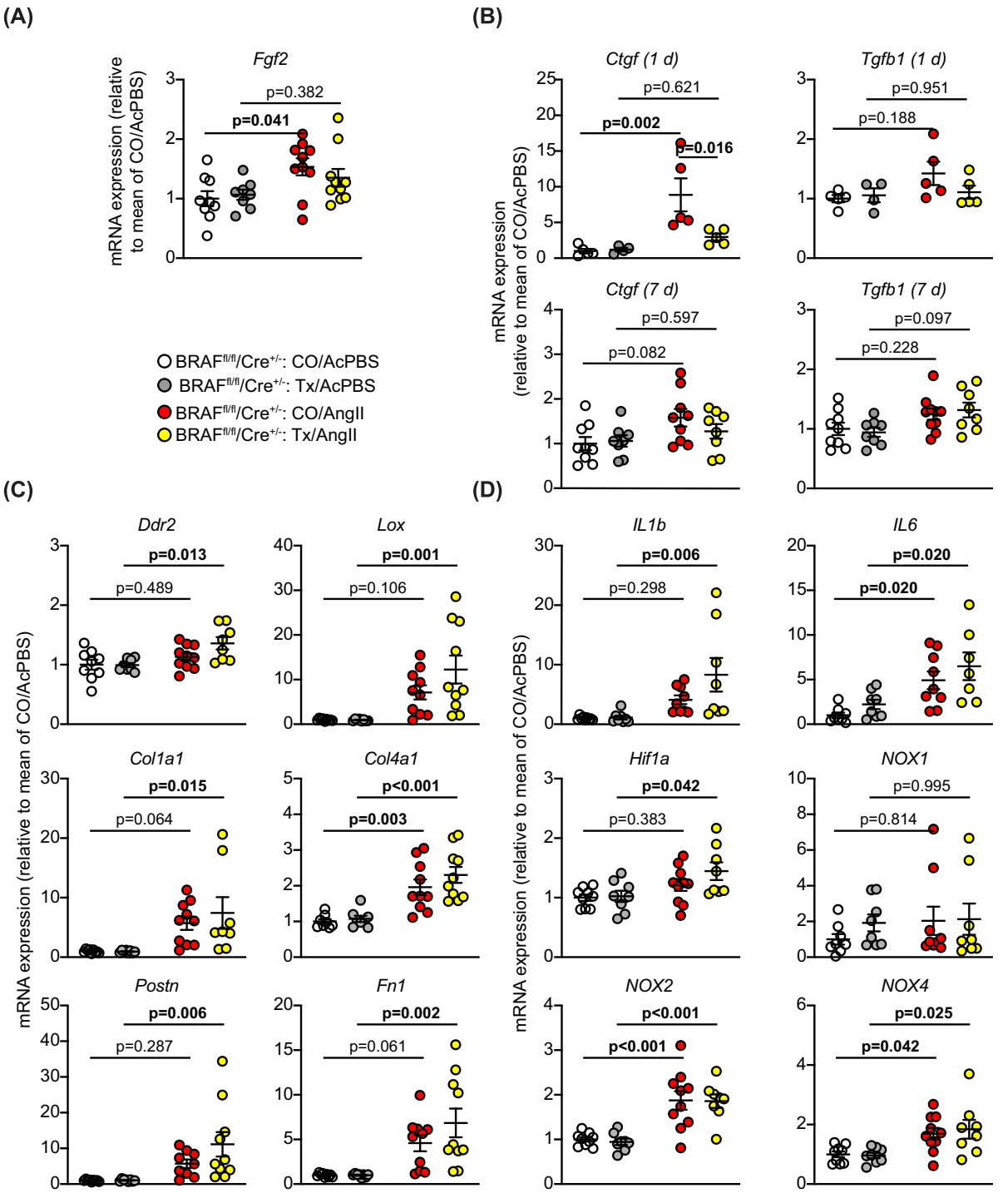

Figure 4. Effects of cardiomyocyte BRAF knockout on changes in mRNA expression induced by AngII in male mouse hearts

Male BRAF$^{fl/fl}$/Cre$^{+/-}$ (BRAF) mice were treated with corn-oil (CO) or tamoxifen in CO (Tx) 4 days before minipumps were implanted to deliver acidified PBS (AcPBS) or 0.8 mg/kg/d AngII in AcPBS (AngII) for 1 or 7 d. RNA was extracted and expression of selected genes assessed by qPCR. (**A**) *Fgf2* was assessed at 7 d. (**B**) *CTGF* and *TGFB1* were assessed at 1 or 7 d as indicated. (**C**) Pro-fibrotic genes (*Ddr2, Lox, Col1a1, Col4a1, Postn, Fn1*) were assessed at 7 d. (**D**) Pro-inflammatory (*IL1b, IL6*) and oxidant (*Hif1a, NOX1, NOX2, NOX4*) genes were assessed at 7 d. Data are presented as individual values with means ± SEM. Statistical analysis used two-way ANOVA with Holm-Sidak's post-test. Statistically significant values ($P<0.05$) are in bold type.

Cardiomyocyte BRAF does not drive cardiomyocyte hypertrophy in response to phenylephrine and suppresses fibrosis in male mice

In contrast with AngII, phenylephrine (as an α_1-adrenergic receptor agonist) is associated with adaptive physiological hypertrophy and, although there are additional systemic effects including effects on blood pressure (see Discussion), it promotes compensated cardiac hypertrophy acting directly on the cardiomyocytes [44]. Male mice were treated with 40 mg/kg/d phenylephrine in PBS or PBS alone (7 d) using osmotic minipumps, implanted 4 d after tamoxifen administration as for AngII (Figure 2A). In contrast with AngII, phenylephrine promoted a significant increase in HW:BW ratio (Supplementary Figure S1A). As in previous studies [29], phenylephrine promoted cardiac hypertrophy as assessed by echocardiography with decreased LV internal diameter and increased wall thickness, and neither appeared to be significantly affected in hearts of mice with cardiomyocyte BRAF knockout (Figure 5A; Supplementary Table S6). In contrast with the effects of AngII (Figure 2E), phenylephrine had no significant effect on mRNA expression of hypertrophic gene markers, and this was not affected by cardiomyocyte BRAF knockout (Figure 5B). Furthermore, the increase in cardiomyocyte cross-sectional area induced by phenylephrine was not significantly reduced by cardiomyocyte BRAF knockout (Figure 5C). This is consistent with our previous studies showing that phenylephrine promotes cardiomyocyte hypertrophy via insulin receptor family members and protein kinase B (PKB, or Akt) [29]. Phenylephrine alone promoted relatively little increase in cardiac fibrosis (Figure 5D,E), particularly compared with AngII (Figure 3A,B). Surprisingly, both perivascular and interstitial fibrosis were significantly and substantially increased in hearts of mice with cardiomyocyte BRAF knockout when treated with phenylephrine, with a particularly striking effect on interstitial fibrosis that in some cases permeated the full cross-sectional area of the myocardium (Figure 5D–F). As with AngII (Figure 3A–C), the effects of cardiomyocyte BRAF knockout on 'physiological' hypertrophy induced by phenylephrine (Figure 5D–F) suggest that the origin of interstitial fibrosis is independent of perivascular fibrosis and controlled to some degree by the cardiomyocytes.

Cardiomyocyte BRAF knockout in female versus male mice: effects on phenylephrine-induced cardiac hypertrophy

There are sex-specific differences in the physiological hypertrophic response of the heart in female versus male animals (e.g. in exercise-induced hypertrophy [45]), probably due in part to sex hormones and influences on metabolism [46]. We therefore assessed the role of cardiomyocyte BRAF in the hypertrophic response to phenylephrine in the female $BRAF^{fl/fl}/Cre^{+/-}$ littermates of the males used in the experiments outlined above. Because of their smaller size, experiments were initiated with female mice at 9–10 weeks of age. The females were still significantly smaller than the males, but (as with the males) there was no significant difference in body weights between the groups of mice with different treatments at baseline or at the end of the experiment (Figure 6A and Supplementary Table S1). Mice were anaesthetized for echocardiography and cardiac function and dimensions were assessed prior to intervention. We detected no significant difference in heart rate, ejection fraction or fractional shortening between male and female hearts, nor was there any difference in global longitudinal or circumferential strain (Figure 6B). Thus, cardiac function was similar in males and females. Stroke volume and cardiac output in female mice was significantly less than the male mice, probably because diastolic LV internal diameter and predicted end diastolic volume were less (though non-significant) with no difference in systolic measurements (Figure 6C). However, predicted end diastolic LV mass was ∼13.8% greater in male mice than in female mice [49.56 ± 0.87 mg (n=31) and 43.56 ± 0.77 mg (n=39), respectively (means ± SEM)] (Figure 6D). This was reflected in the significant difference in diastolic and systolic LV wall thickness. There was no evidence for recombination in female or male hearts in the absence of tamoxifen, and treatment with tamoxifen induced a similar degree of recombination (and therefore cardiomyocyte BRAF knockout) in females as in males (Figure 6E). Treatment with tamoxifen resulted in a decrease in BRAF protein but, unlike the males, we did not detect any decrease in RAF1 protein (Figure 6F). There was no difference between males and females in expression of ERK1/2 or the level of the activating phosphorylations (Figure 6G,H).

Female $BRAF^{fl/fl}/Cre^{+/-}$ mice were treated with 40 mg/kg tamoxifen or corn-oil vehicle, and then minipumps were implanted for delivery of 40 mg/kg/d phenylephrine using the same schedule as for male mice (Figure 2A). Unlike in male mice, phenylephrine alone did not increase HW:BW ratio in female mice, although there was an increase with cardiomyocyte BRAF knockout (Supplementary Figure S1B). Over 7 d, phenylephrine promoted cardiac hypertrophy as assessed by echocardiography in the female mice with a decrease in internal diameter and increase in LV wall thickness as assessed using M-mode imaging of the short axis view of the heart (Figure 7A and Supplementary Table S7). Peripheral cardiomyocytes were smaller in female hearts than in male hearts, and the increase in cross-sectional area induced by phenylephrine was significant, but less than that detected in male hearts (Figures 5C and 7B). Tamoxifen treatment and BRAF knockout resulted in a small decrease in cardiomyocyte size in the female hearts and

Clinical Science (2022) **136** 1661–1681
https://doi.org/10.1042/CS20220607

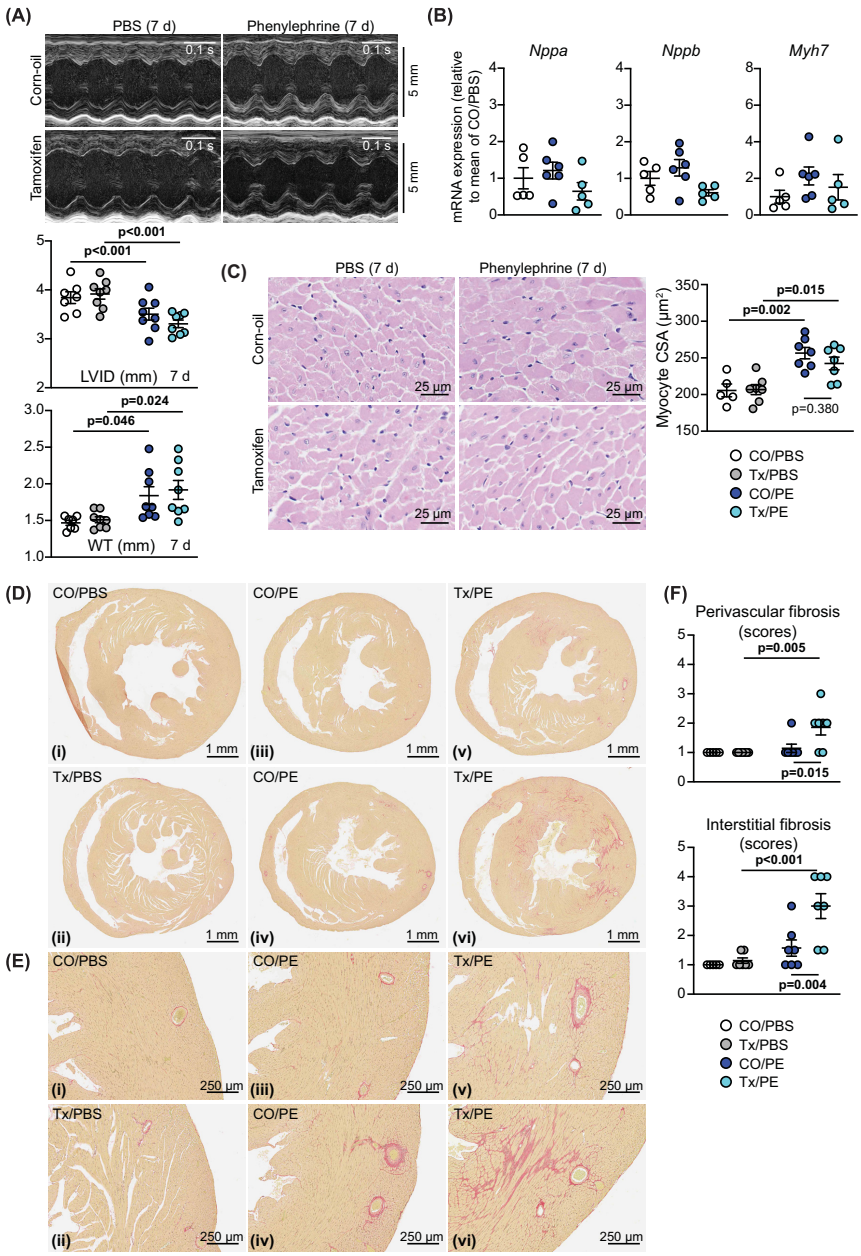

Figure 5. Cardiomyocyte BRAF knockout does not inhibit cardiomyocyte hypertrophy induced by phenylephrine in male mouse hearts but increases cardiac fibrosis

Male BRAF$^{fl/fl}$/Cre$^{+/-}$ mice were treated with corn-oil (CO) or tamoxifen in CO (Tx) 4 days before minipumps were implanted to deliver PBS or 40 mg/kg/d phenylephrine in PBS (PE) for 7 d. (**A**) Representative M-mode echocardiograms taken from short axis views of the heart (upper panels) with analysis of echocardiograms to assess cardiac dimensions (lower panels). Abbreviations: LVID, left ventricle internal diameter; WT, left ventricle wall thickness (posterior plus anterior walls). Diastolic measurements are shown. (**B**) mRNA expression in mouse hearts after 7 d treatment with phenylephrine. (**C**) Haematoxylin and eosin staining of mouse heart sections (left panels) with assessment of cardiomyocyte cross-sectional area (CSA; right panel). Images and measurements are from the periphery of the left ventricle. (**D,E**) Picrosirius red staining of mouse heart sections showing short axis views of the whole heart (D) with enlarged sections (E) from the same views (the red stain shows accumulation of fibrotic material). Representative (average) images are shown for mice treated with CO/PBS (i), Tx/PBS (ii), CO/PE (iii) and Tx/PE (v). Additional images are shown for the most severe degree of fibrosis with CO/PE (iv) and Tx/PE (vi). (**F**) Quantification of fibrosis. This was scored as: 1 = the least amount of fibrosis; 2 = low level fibrosis; 3 = high level fibrosis in at least one area of the myocardium; 4 = high level fibrosis throughout the myocardium (half scores were used). Data are presented as individual values with means ± SEM. Statistical analysis used two-way (A,C,F) or one-way (B) ANOVA with Holm-Sidak's post-test. Statistically significant values ($P<0.05$) are in bold type.

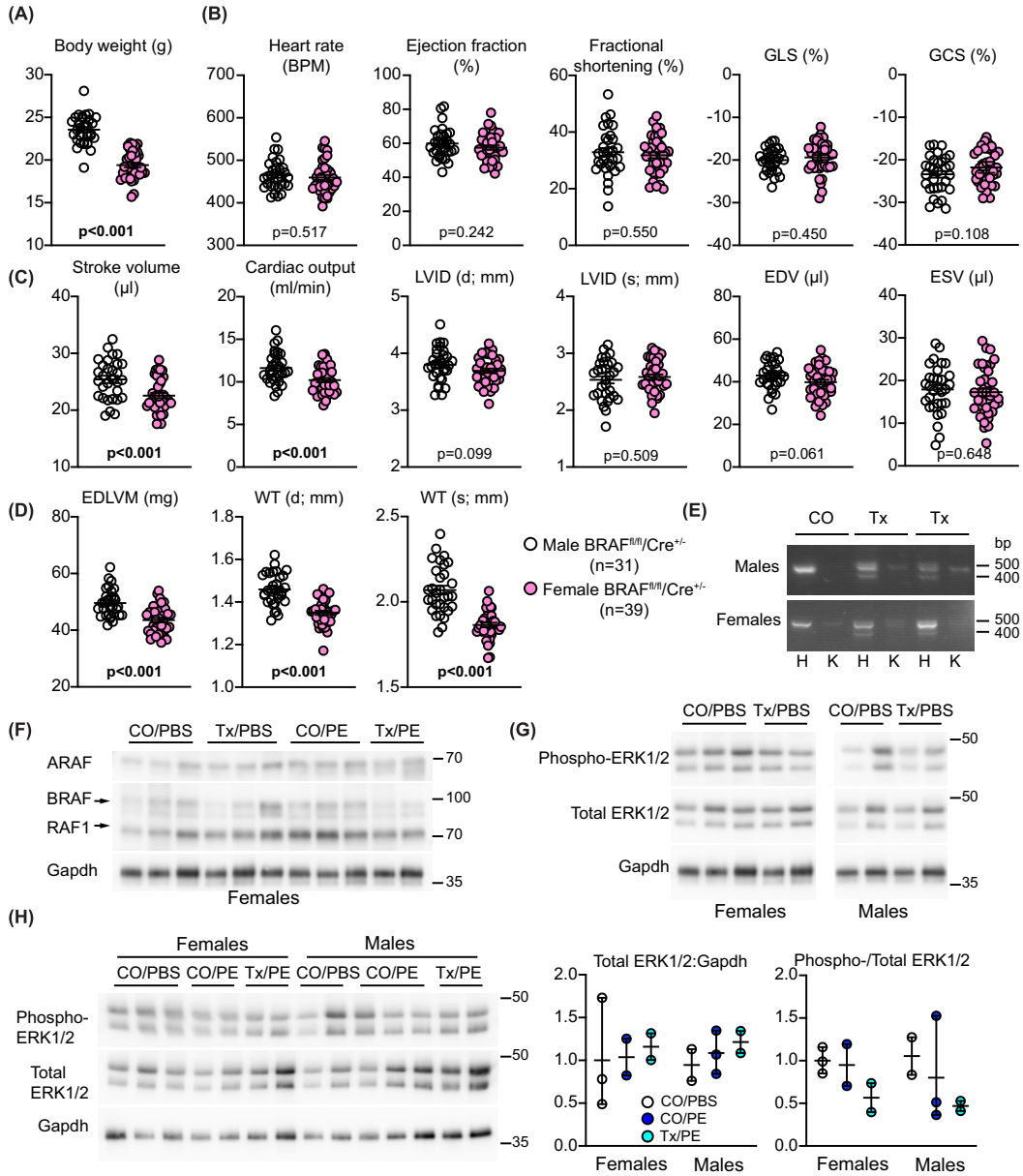

Figure 6. Comparison of cardiac function/dimensions and confirmation of recombination in female BRAF$^{fl/fl}$/Cre$^{+/-}$ mice compared with male littermates

(**A–D**) Data were gathered from mice at the time of the first baseline echocardiogram taken from male and female BRAF$^{fl/fl}$/Cre$^{+/-}$ littermates (males: 7–8 weeks; females: 9–10 weeks). (A) Body weights. (B) Heart rate, ejection fraction and fractional shortening, global longitudinal strain (GLS) and global circumferential strain (GCS) were measured from B-mode images of long-axis views using VevoStrain speckle-tracking software. (**C,D**) Stroke volume, cardiac output, end diastolic volume (EDV), end systolic volume (ESV) and end diastolic LV mass (EDLVM) were measured from B-mode images of long-axis views using VevoStrain speckle-tracking software. Diastolic (d) and systolic (s) left ventricle (LV) internal diameter (ID) and wall thickness (WT: anterior plus posterior walls) measurements were measured from M-mode images of short axis views using VevoLab software. (**E**) Confirmation of recombination using cDNA prepared from RNA extracted from the hearts of male (upper image) and female (lower image) littermates 11 d post-tamoxifen treatment. PCR amplification used forward primers in exon 9 with reverse primers in exon 13. Deletion of exon 12 in cardiomyocytes resulted in the appearance of a smaller product in heart (**H**) but not kidney (**K**) of mice treated with tamoxifen (Tx) in corn-oil (CO) but not CO alone. Representative images are shown. (**F–H**) Immunoblot analysis of RAF isoforms (F) or phosphorylated and total ERK1/2 (G,H) in relation to Gapdh in samples of female or male (as indicated) mouse hearts treated with CO or Tx 4 days before administration of phenylephrine (PE) in PBS or PBS alone for 7 d. Representative immunoblots are shown. Densitometric analysis of the blots in H are in the right panels. Individual data points are shown with the mean and range.

Clinical Science (2022) **136** 1661–1681
https://doi.org/10.1042/CS20220607

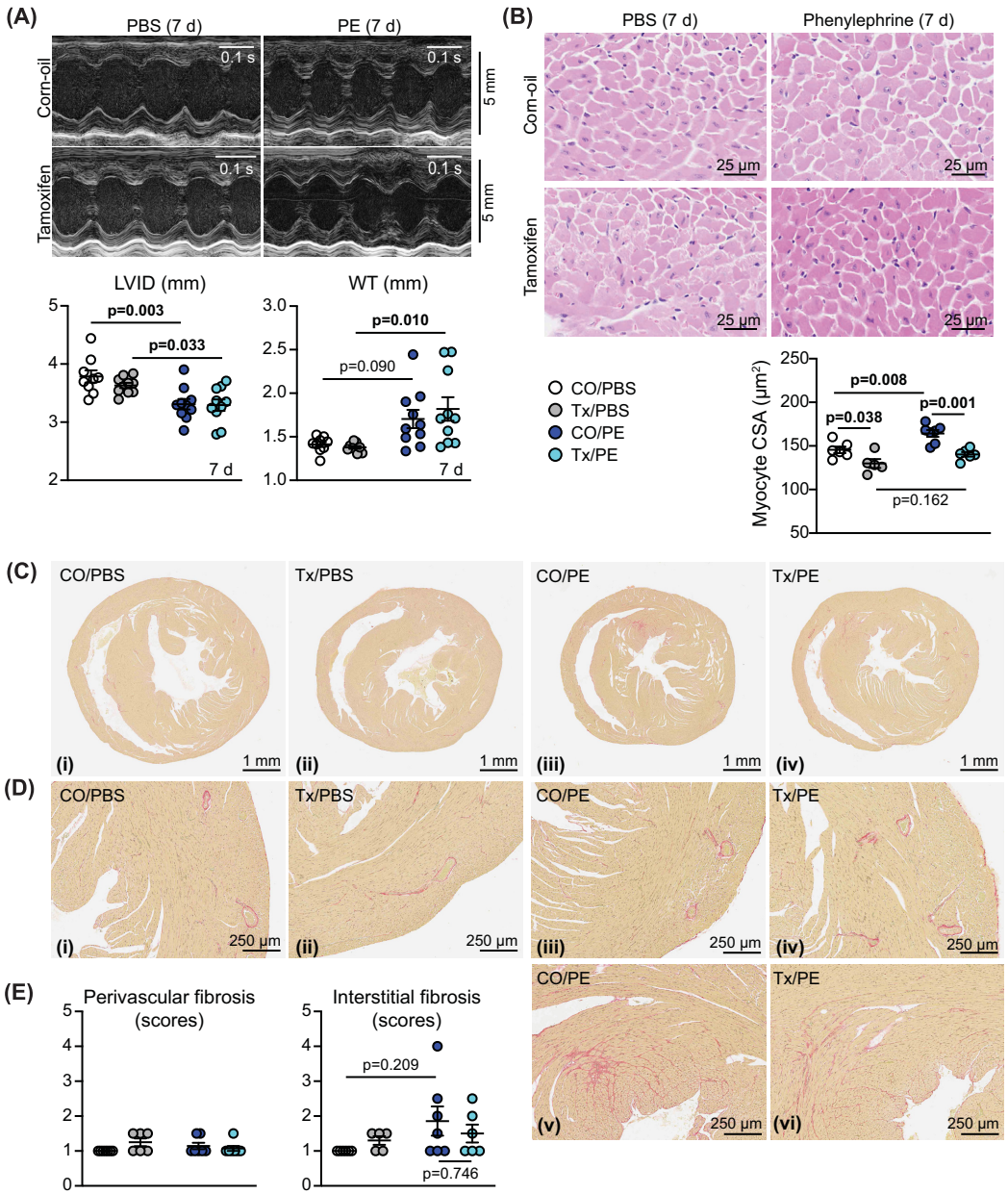

Figure 7. Assessment of the effects of cardiomyocyte BRAF knockout on the response of female mouse hearts to phenylephrine

Female BRAF$^{fl/fl}$/Cre$^{+/-}$ mice were treated with corn-oil (CO) or tamoxifen in CO (Tx) 4 days before minipumps were implanted to deliver PBS or 40 mg/kg/d phenylephrine in PBS (PE) for 7 d. (**A**) Representative M-mode echocardiograms taken from short axis views of the heart (upper panels) with analysis of echocardiograms to assess cardiac dimensions (lower panels). Abbreviations: LVID, left ventricle internal diameter; WT, left ventricle wall thickness (posterior plus anterior walls). Measurements were taken at diastole. (**B**) Haematoxylin and eosin staining of mouse heart sections (upper panels) with assessment of cardiomyocyte cross-sectional area (CSA; lower panel). Images and measurements are from the periphery of the left ventricle. (**C,D**) Picrosirius red staining of mouse heart sections showing short axis views of the whole heart (C) with enlarged sections (D) from the same views (the red stain shows accumulation of fibrotic material). Representative (average) images are shown for mice treated with CO/PBS (i), Tx/PBS (ii), CO/PE (iii) and Tx/PE (iv). Additional images are shown for the most severe degree of fibrosis with CO/PE (v) and Tx/PE (vi). (**E**) Quantification of fibrosis. This was scored as: 1 = the least amount of fibrosis; 2 = low level fibrosis; 3 = high level fibrosis in at least one area of the myocardium; 4 = high level fibrosis throughout the myocardium (half scores were used). Data are presented as individual values with means ± SEM. Statistical analysis used two-way ANOVA with Holm-Sidak's post-test. Statistically significant values ($P<0.05$) are in bold type.

the minor increase in cardiomyocyte size induced by phenylephrine was less apparent (Figure 7B). Phenylephrine increased interstitial fibrosis in some female hearts, particularly in focal areas, but (unlike male hearts) fibrosis was not enhanced with cardiomyocyte BRAF knockout (Figure 7C–E). In contrast with male hearts, there was no significant effect on perivascular fibrosis. Overall, the response of female mouse hearts to phenylephrine without or with cardiomyocyte BRAF knockout differed from that of the male counterparts. This did not appear to relate to ERK1/2 signalling with no effect on the level of phosphorylated ERK1/2 in male or female mice, although phenylephrine increased expression of total ERK1/2 in parallel with Gapdh (Figure 6H).

Increasing interstitial fibrosis causes stiffening of the myocardium which leads to diastolic dysfunction. These changes are not necessarily detected using standard M-mode or B-mode echocardiography. Since strain analysis is potentially more sensitive [47], we analysed B-mode images from the phenylephrine study using speckle-tracking software, comparing hearts from male and female mice (Figure 8A,B, representative images shown for 7 d only; Supplementary Tables S6 and S7). This approach detected greater baseline variation between animals, so we compared the data obtained at 7 d with baseline data for each mouse individually using paired two-way ANOVA with Holm-Sidak's post-test. Heart rate and stroke volumes were unaffected by phenylephrine treatment with or without cardiomyocyte BRAF knockout (Figure 8C,D). Consistent with M-mode imaging, phenylephrine promoted a decrease in end diastolic volume and increased end diastolic LV mass in males and females, an effect that was not affected by cardiomyocyte BRAF knockout (Figure 8E,F). As with M-mode imaging, there was greater variation in the response of the females and the overall increase in LV mass was relatively less than in males. The lesser degree of hypertrophy induced in female hearts by phenylephrine became apparent in measures of ejection fraction and fractional shortening, in addition to global longitudinal and circumferential strain, all of which were increased by phenylephrine in males, but not females (Figure 8G–J). In the males, significant changes were not induced by phenylephrine in hearts with cardiomyocyte BRAF knockout (Figure 8G,I), consistent with the adaptive response being compromised with respect to cardiac function, presumably a result of the increase in interstitial fibrosis (Figure 5D–F). Surprisingly, in female mice with phenylephrine, cardiomyocyte BRAF knockout resulted in an increase in ejection fraction and fractional shortening, along with increased circumferential strain (Figure 8H,J). The reasons are not clear, but the data indicate that BRAF signalling has a different effect in female myocytes than in male myocytes and loss of cardiomyocyte BRAF enhances contractile function.

Discussion

Cardiac hypertrophy is generally considered a predisposing risk factor for heart failure, but cardiomyocyte hypertrophy is a necessary and important adaptation that allows the adult heart to accommodate any increase in workload whether physiological as with exercise or pregnancy, or pathological as with hypertension. Here, we have studied the early adaptive phase, particularly focusing on the response of male mouse hearts to the hypertensive agent AngII compared with a more physiological form of hypertrophy induced by phenylephrine. Both caused hypertrophy with reduced LV internal diameter and increased LV wall thickness and mass, but the aetiology is quite different, along with the influence of cardiomyocyte BRAF. We did not measure blood pressure in this study. However, the concentrations of AngII and phenylephrine that we selected would have had a limited effect on blood pressure over the 7 d period studied here. The concentration of AngII (0.8 mg/kg/d) is a slow pressor dose that gradually induces hypertension over 7–14 days, having a limited effect at 7 d (as in [27]). Others use higher doses with a more immediate pressor effect (e.g. >2 mg/kg/d [7]) that can be associated with sudden cardiac death. In our hands, concentrations of even 1 mg/kg/d caused sudden cardiac death in 10–30% of mice within 3 d, presumably because of the immediate pressor effect (data not shown). In our studies of phenylephrine, we used a relatively high dose (40 mg/kg/d) as in [29]. This may increase blood pressure but, as in other studies of male mice with a similar level of dosage (27 mg/kg/d [30]), the increase over 7 d is likely to be limited to <10%. Thus, the effects of the AngII and PE in this study are most probably a direct result of receptor stimulation in the heart rather than necessarily an overt effect of increasing blood pressure.

In hypertension, even though cardiomyocytes may themselves possess mechanosensors such as stretch-regulated ion channels [36], the primary effect is on the arterioles and the endothelial cells lining the blood vessels in the heart. These cells also possess AngII receptors and so are stimulated directly by this treatment and, as discussed above, this is most likely to be the primary effect in this study. This was clearly seen in the histology, with a striking and dominant effect of AngII on perivascular fibrosis around the arterioles (Figure 3A–C). It is likely that endothelial or smooth muscle cells in the walls of the arterioles produce neurohumoral factors (e.g. endothelin-1 [38]) which then stimulate cardiomyocyte hypertrophy. These act through the various signalling pathways including the ERK1/2 cascade to promote changes in gene and protein expression, including increased expression of growth factors. Our data show that AngII promoted up-regulation of *Edn1* and *Fgf2* (as an example of a pro-fibrotic growth factor), with

Clinical Science (2022) **136** 1661–1681
https://doi.org/10.1042/CS20220607

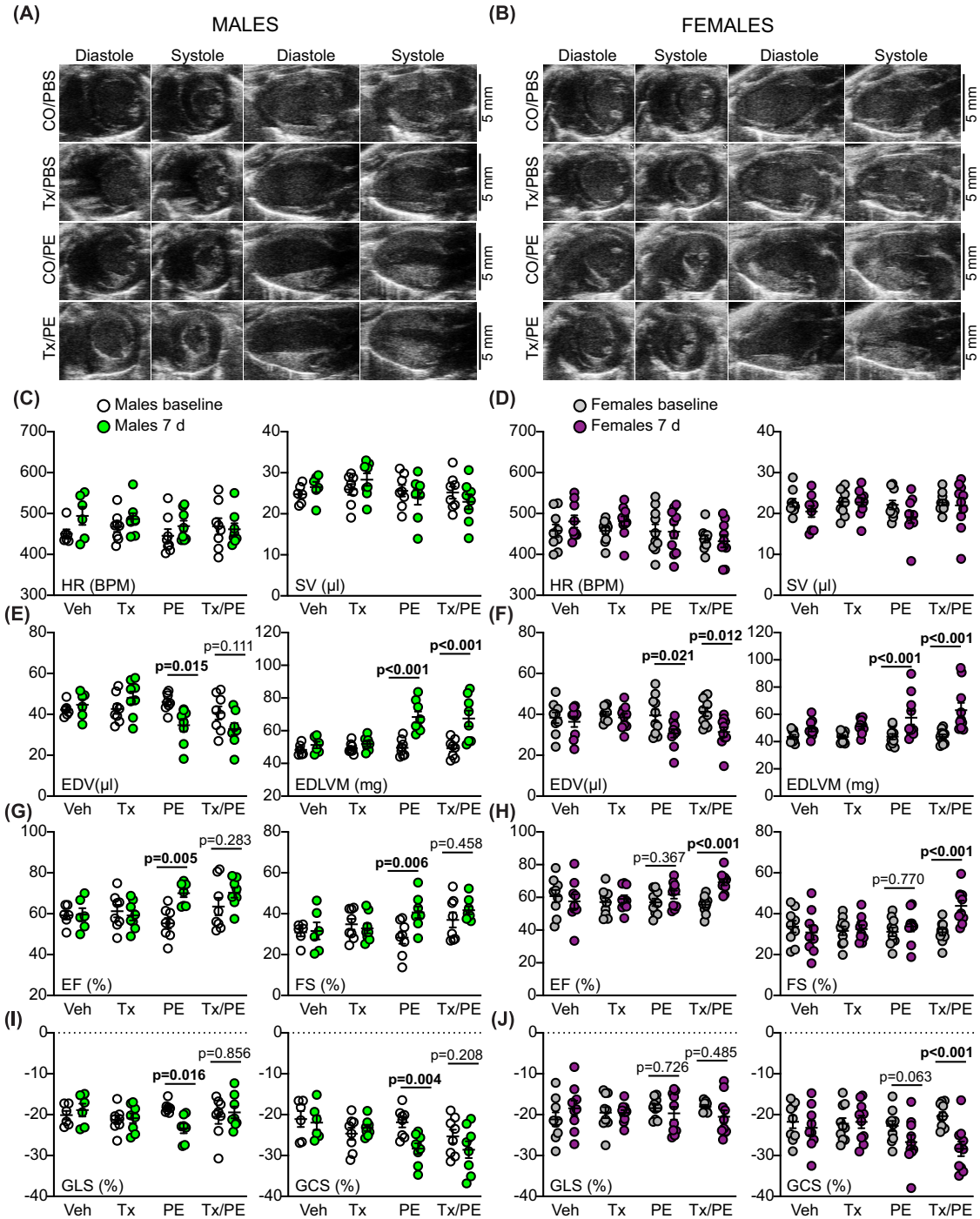

Figure 8. Comparison of effects of cardiomyocyte BRAF knockout on cardiac function in male and female hearts

Male and female BRAF$^{fl/fl}$/Cre$^{+/-}$ mice were treated with CO or tamoxifen in CO (Tx) 4 days before minipumps were implanted to deliver PBS (PBS) or 40 mg/kg/d phenylephrine in PBS (PE) for 7 d. (**A,B**) Representative images are shown for short axis (left two panels) and long axis (right two panels) views in diastole or systole in male (A) or female mice (B). (**C–J**) B-mode images were analysed with VevoStrain speckle-tracking software. (C,D) Heart rate (HR) and stroke volume (SV). (E,F) End diastolic volume (EDV) and end diastolic left ventricle mass (EDLVM). (G,H) Ejection fraction (EF) and fractional shortening (FS). (I,J) Global longitudinal strain (GLS) and global circumferential strain (GCS). (C,E,G,I) Data for male mice; (D,F,H,J) Data for female mice. All parameters except GCS were measured from long axis views; GCS was taken from short axis views. Data are individual values with means ± SEM. Statistical analysis used paired two-way ANOVA with Holm-Sidak's post-test. Statistically significant values ($P<0.05$) are in bold type.

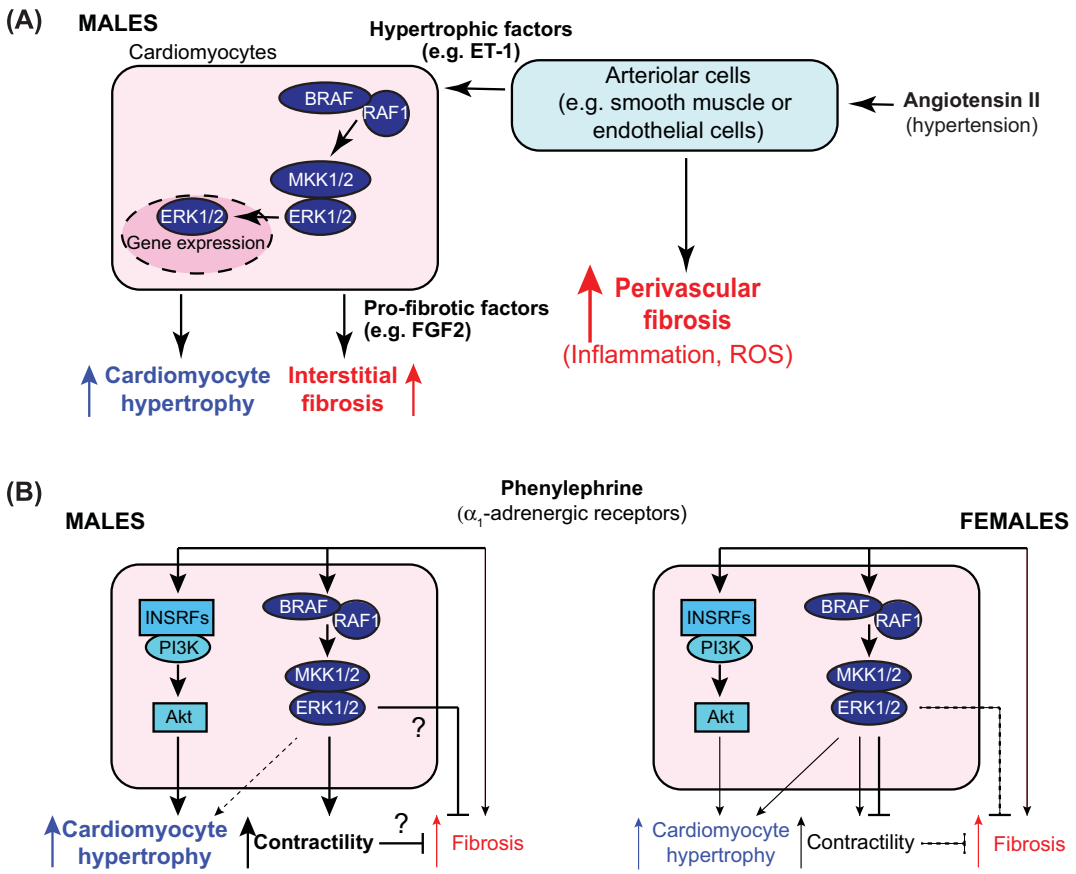

Figure 9. Schematic representations of the conclusions from this study

(**A**) AngII causes hypertension and directly stimulates cells in the walls of cardiac arterioles (e.g. endothelial cells or smooth muscle cells). Acutely (over 7 d), this resulted in perivascular fibrosis around arterioles, along with markers of inflammation and increased ROS. These cells also produced hypertrophic factors such as endothelin-1 (ET-1) that stimulate cardiomyocyte hypertrophy via BRAF/RAF1, MKK1/2 and ERK1/2. Cardiomyocyte hypertrophy was associated with production of pro-fibrotic factors such as fibroblast growth factor 2 (FGF2) downstream of BRAF/RAF1→ERK1/2 signalling, and these increased interstitial fibrosis, probably acting on resident fibroblasts. Loss of BRAF resulted in decreased cardiomyocyte hypertrophy and interstitial, but not perivascular, fibrosis. (**B**) Phenylephrine acts directly on cardiomyocytes in the heart but has some additional systemic effects that may lead to limited cardiac fibrosis. In male mice (left), phenylephrine causes cardiomyocyte hypertrophy acting primarily via insulin receptor family members (INSRFs) and Akt (as described in [29]). BRAF/RAF1→ERK1/2 signalling increased contractility and this increase was lost with cardiomyocyte BRAF knockout. In addition, cardiomyocyte BRAF knockout resulted in increased fibrosis, possibly due to loss of a direct inhibitory signal or because of an imbalance between hypertrophy and contractility. In female mice (right), phenylephrine had a modest effect on cardiomyocyte hypertrophy, possibly with some signal from the ERK1/2 cascade, but did not significantly affect contractility. Cardiomyocyte BRAF knockout increased contractility, possibly due to loss of an inhibitory signal, but there was no effect on fibrosis.

the latter inhibited by cardiomyocyte BRAF knockout suggesting it (but not *Edn1*) originated in the cardiomyocyte (Figures 2F and 3D). FGF2 is likely to stimulate cardiac non-myocytes including resident fibroblasts, and factors such as this are probably responsible for the increase in interstitial fibrosis in this model (Figure 9A). In this scenario, loss of BRAF signalling is predicted to reduce cardiomyocyte hypertrophy and interstitial fibrosis as, indeed, it does.

As an α_1-adrenergic receptor agonist phenylephrine acts directly on cardiomyocytes to promote hypertrophy (Figure 9B), but the signal to hypertrophy is propagated by transactivation of one or more of the insulin receptor family, signalling via PI3K and PKB/Akt rather than ERK1/2 [29]. Consistent with this, cardiomyocyte BRAF knockout did not significantly affect the increase in cardiomyocyte cross-sectional area induced in male mouse hearts by phenylephrine (Figures 5B and 9B). Phenylephrine increased ejection fraction which may be partly attributed to

Clinical Science (2022) **136** 1661–1681
https://doi.org/10.1042/CS20220607

the change in dimensions but also increased cardiac contractility with increased fractional shortening and longitudinal/circumferential strain, an effect which was lost with cardiomyocyte BRAF knockout (Figure 8G,I). Thus, although BRAF signalling may not drive the increase in size in response to phenylephrine, it still influences cardiomyocyte function. This may be mediated by changes in gene expression, but could result from non-genomic effects of ERK1/2 signalling on ion fluxes in the cell. For example, the sodium proton exchanger NHE1 is phosphorylated by p90 ribosomal S6 kinases, downstream of BRAF and the ERK1/2 cascade. This alters the activation profile of NHE1 and is associated with increased contractility [48,49]. Notably, expression of activated NHE1 in mice enhances the degree of hypertrophy induced by phenylephrine [50] suggesting that it is a contributing factor to the overall response. The other effect of cardiomyocyte BRAF knockout in male mice was to increase cardiac fibrosis, particularly interstitial fibrosis (Figure 5D–F). The mechanism is not clear, but could derive from loss of a BRAF signal to inhibit fibrosis, possibly an element of the known cytoprotective aspect of ERK1/2 signalling. Alternatively, it could result from the imbalance resulting from sustained cardiomyocyte hypertrophic growth in a context of compromised contractility. On the other hand, increased fibrosis may be expected to compromise contractility but sustain cardiomyocyte hypertrophy. This interplay between the pro-hypertrophic signalling from PI3K-PKB/Akt and the ERK1/2 cascade clearly requires further study.

Overall, BRAF emerged as a key signalling intermediate in male mice, in the development of both pathological hypertrophy where it has a direct effect on cardiomyocyte size and in physiological hypertrophy to prevent accumulation of fibrotic material during remodelling of the heart. The role of BRAF in cardiomyocytes differs from RAF1 which is potently cytoprotective [19]. This may appear anomalous since our data also show that BRAF and RAF1 exist as preformed heterodimers in cardiomyocytes [16] and they might be expected to have the same role. However, not all RAF1 associates with BRAF, and RAF1 phosphorylates and inhibits pro-apoptotic kinases [16,51,52]. There seem to be no reports of the roles of other MKK1/2 activating kinases, ARAF and Tpl2/Cot, in the heart although both are expressed in cardiomyocytes [18]. ARAF may be a partner for RAF1 in cytoprotection, whilst Tpl2/Cot is probably important in the inflammatory response, but further studies could reveal additional specific roles for these kinases.

Despite the increasing appreciation of the importance of heart failure in women, there are still relatively few preclinical studies comparing the responses of male and female hearts. This study highlights the importance of research in this area. Even in the absence of any intervention, there were clear differences in cardiac dimensions that were not simply due to the difference in body weight (Figure 6A–D). The smaller LV internal diameter and LV volume resulted in a significant decrease in stroke volume and cardiac output, and the myocardial walls were significantly thinner. Despite this, although measured under anaesthetic, heart rates, ejection fraction and fractional shortening were similar in males and females. Apart from differences at baseline, female hearts exhibited a different response to phenylephrine (Figure 9B), and the degree of hypertrophy, though significant, was less pronounced (Figure 7). The functional effects were also different, with little or no increase in contractility (Figure 8H,J). We currently have no explanation for these differences given the relative paucity of data on female mouse heart function.

Our model (like many) used a system for inducible gene manipulation using a form of Cre that is activated by tamoxifen. In contrast with the male hearts, tamoxifen treatment in female mice had a small, but significant inhibitory effect on cardiomyocyte size (Figure 7B). Even though the tamoxifen should have cleared the body within 2–3 d of administration [32], the pharmacokinetics in females and in this particular line of mice may differ and there could still be residual effects at the end of the experiment (11 d post-injection). Since tamoxifen is an antagonist for oestrogen and oestrogen promotes PKB/Akt signalling in female hearts [53,54], it is feasible that the decrease in cardiomyocyte cross-sectional area is due entirely to the effects of tamoxifen. However, it is equally likely that cardiomyocyte BRAF knockout caused the reduction in cardiomyocyte cross-sectional area. Further studies will be necessary to dissect this, probably in parallel with the role of the PI3K→PKB/Akt pathway and insulin receptor family signalling that plays a significant role in male hearts [29]. Perhaps it should also be considered that a different type of cell-specific and inducible genetic system is required for females that does not use tamoxifen and which can also be used in males.

The implications of this study extend beyond just the understanding of the role of cardiomyocyte BRAF in the two models of hypertrophy shown. Not least, our study raises questions about the development of hypertrophy and heart failure in females compared with males, along with the most appropriate systems for studying gene function in females. Clearly, independent and thorough investigation of the responses of the female heart and the roles of individual genes are urgently needed. Nevertheless, BRAF remains a significant therapeutic target for cancer [55] and our data show that it is an important regulator of cardiac hypertrophy at least in male mice. Because existing drugs can activate RAF signalling in cancer cells through the RAF 'paradox' [12], other types of inhibitor are in development for more robust inhibition of RAF kinases (e.g. Type 2 inhibitors and BRAF-PROTAC degraders that target BRAF to the proteosome) [55]. Such drugs seem unlikely to have overt on-target cardiotoxic effects in patients without cardiovascular complications (since cardiomyocyte BRAF knockout alone did not affect cardiac function and

dimensions), although there may be some risk for patients with underlying cardiac hypertrophy that requires BRAF signalling. On the other hand, BRAF inhibitors may be beneficial in, for example, hypertensive heart disease to reduce interstitial fibrosis. Further studies of cross-talk between different cardiac cell types may provide additional insight and identify new therapeutic approaches to manage fibrosis in the heart.

Clinical perspectives

- Background. BRAF is a key signalling intermediate that causes cancer and is up-regulated in heart failure, but its role in physiological and pathological cardiac hypertrophy remains to be established.
- Summary. Cardiomyocyte BRAF is required in male mice for hypertrophy and contributes to interstitial fibrosis in hypertension induced by AngII, but it increases contractility and suppresses fibrosis in physiological hypertrophy induced by α_1-adrenergic receptor stimulation with phenylephrine. Differences between males and females are highlighted in the phenylephrine response.
- Potential significance of results to human health and disease. BRAF is a key signalling node in both pathological and physiological hypertrophy: inhibiting BRAF may be beneficial in pathological hypertrophy and the data have implications for repurposing of RAF inhibitors developed for cancer; inhibiting BRAF in physiological hypertrophy may result in increased fibrosis and using RAF inhibitors in this context could be detrimental in the longer term.

Data Availability

All primary data are available from the corresponding author upon reasonable request. Additional data sharing information is not applicable to this study.

Competing Interests

The authors declare that there are no competing interests associated with the manuscript.

Funding

This work was funded by Qassim University, Saudi Arabia (to H.O.A) and the British Heart Foundation [grant numbers PG/13/71/30460, PG/17/11/32841, FS/18/33/33621, PG/15/24/31367 and FS/19/24/34262].

Ethics Approval

All procedures were performed in accordance with U.K. regulations and the European Parliament Directive 2010/63/EU for animal experiments. This work was undertaken in accordance with local institutional animal care committee procedures at University of Reading and St. George's University of London, and the U.K. Animals (Scientific Procedures) Act 1986. Studies were conducted under Project Licences 70/8249 (University of Reading) and P8BAB0744 (both institutions).

CRediT Author Contribution

Hajed O. Alharbi: Data curation, Formal analysis, Investigation, Methodology. **Michelle A. Hardyman:** Data curation, Formal analysis, Investigation, Methodology. **Joshua J. Cull:** Investigation, Methodology. **Thomais Markou:** Investigation, Methodology. **Susanna T.E. Cooper:** Investigation. **Peter E. Glennon:** Supervision, Methodology. **Stephen J. Fuller:** Conceptualization, Supervision, Investigation, Methodology. **Peter H. Sugden:** Conceptualization, Formal analysis, Writing—original draft, Writing—review & editing. **Angela Clerk:** Conceptualization, Resources, Data curation, Formal analysis, Supervision, Funding acquisition, Investigation, Methodology, Writing—original draft, Project administration, Writing—review & editing.

Acknowledgements

We thank Andrew Cripps, Mhairi Baxter and Wayne Knight (University of Reading), and Robert Bond, Emma Mustafa and Rene Ocho (St. George's University of London) for support for the *in vivo* mouse studies.

Clinical Science (2022) **136** 1661–1681
https://doi.org/10.1042/CS20220607

Abbreviations

AngII, Angiotensin II; ERK1/2, extracellular signal-regulated kinase 1/2; ET-1, endothelin-1; FGF2, fibroblast growth factor 2; GLS, global longitudinal strain; MAPK, mitogen-activated protein kinase; LV, left ventricle; ROS, reactive oxygen species.

References

1 Dorn, II, G.W., Robbins, J. and Sugden, P.H. (2003) Phenotyping hypertrophy: eschew obfuscation. *Circ. Res.* **92**, 1171–1175, https://doi.org/10.1161/01.RES.0000077012.11088.BC
2 Tarone, G., Balligand, J.L., Bauersachs, J., Clerk, A., de Windt, L., Heymans, S. et al. (2014) Targeting myocardial remodelling to develop novel therapies for heart failure: A position paper from the Working Group on Myocardial Function of the European Society of Cardiology. *Eur. J. Heart Fail.* **16**, 494–508, https://doi.org/10.1002/ejhf.62
3 Sugden, P.H. and Clerk, A. (1998) Cellular mechanisms of cardiac hypertrophy. *J. Mol. Med. (Berl.)* **76**, 725–746, https://doi.org/10.1007/s001090050275
4 Rose, B.A., Force, T. and Wang, Y. (2010) Mitogen-activated protein kinase signaling in the heart: angels versus demons in a heart-breaking tale. *Physiol. Rev.* **90**, 1507–1546, https://doi.org/10.1152/physrev.00054.2009
5 Kehat, I. and Molkentin, J.D. (2010) Extracellular signal-regulated kinase 1/2 (ERK1/2) signaling in cardiac hypertrophy. *Ann. N.Y. Acad. Sci.* **1188**, 96–102, https://doi.org/10.1111/j.1749-6632.2009.05088.x
6 Thum, T., Gross, C., Fiedler, J., Fischer, T., Kissler, S., Bussen, M. et al. (2008) MicroRNA-21 contributes to myocardial disease by stimulating MAP kinase signalling in fibroblasts. *Nature* **456**, 980–984, https://doi.org/10.1038/nature07511
7 Schafer, S., Viswanathan, S., Widjaja, A.A., Lim, W.W., Moreno-Moral, A., DeLaughter, D.M. et al. (2017) IL-11 is a crucial determinant of cardiovascular fibrosis. *Nature* **552**, 110–115, https://doi.org/10.1038/nature24676
8 Bueno, O.F., De Windt, L.J., Tymitz, K.M., Witt, S.A., Kimball, T.R., Klevitsky, R. et al. (2000) The MEK1-ERK1/2 signaling pathway promotes compensated cardiac hypertrophy in transgenic mice. *EMBO J.* **19**, 6341–6350, https://doi.org/10.1093/emboj/19.23.6341
9 Lips, D.J., Bueno, O.F., Wilkins, B.J., Purcell, N.H., Kaiser, R.A., Lorenz, J.N. et al. (2004) MEK1-ERK2 signaling pathway protects myocardium from ischemic injury in vivo. *Circulation* **109**, 1938–1941, https://doi.org/10.1161/01.CIR.0000127126.73759.23
10 Purcell, N.H., Wilkins, B.J., York, A., Saba-El-Leil, M.K., Meloche, S., Robbins, J. et al. (2007) Genetic inhibition of cardiac ERK1/2 promotes stress-induced apoptosis and heart failure but has no effect on hypertrophy in vivo. *Proc. Natl. Acad. Sci. U.S.A.* **104**, 14074–14079, https://doi.org/10.1073/pnas.0610906104
11 Kehat, I., Davis, J., Tiburcy, M., Accornero, F., Saba-El-Leil, M.K., Maillet, M. et al. (2011) Extracellular signal-regulated kinases 1 and 2 regulate the balance between eccentric and concentric cardiac growth. *Circ. Res.* **108**, 176–183, https://doi.org/10.1161/CIRCRESAHA.110.231514
12 Durrant, D.E. and Morrison, D.K. (2018) Targeting the Raf kinases in human cancer: the Raf dimer dilemma. *Br. J. Cancer* **118**, 3–8, https://doi.org/10.1038/bjc.2017.399
13 Roskoski, Jr, R. (2018) Targeting oncogenic Raf protein-serine/threonine kinases in human cancers. *Pharmacol. Res.* **135**, 239–258, https://doi.org/10.1016/j.phrs.2018.08.013
14 Matallanas, D., Birtwistle, M., Romano, D., Zebisch, A., Rauch, J., von Kriegsheim, A. et al. (2011) Raf family kinases: old dogs have learned new tricks. *Genes Cancer* **2**, 232–260, https://doi.org/10.1177/1947601911407323
15 Rauch, J. and Kolch, W. (2019) Spatial regulation of ARAF controls the MST2-Hippo pathway. *Small GTPases* **10**, 243–248
16 Clerk, A., Meijles, D.N., Hardyman, M.A., Fuller, S.J., Chothani, S.P., Cull, J.J. et al. (2022) Cardiomyocyte BRAF and type 1 RAF inhibitors promote cardiomyocyte and cardiac hypertrophy in mice in vivo. *Biochem. J.* **479**, 401–424, https://doi.org/10.1042/BCJ20210615
17 Bogoyevitch, M.A., Marshall, C.J. and Sugden, P.H. (1995) Hypertrophic agonists stimulate the activities of the protein kinases c-Raf and A-Raf in cultured ventricular myocytes. *J. Biol. Chem.* **270**, 26303–26310, https://doi.org/10.1074/jbc.270.44.26303
18 Fuller, S.J., Osborne, S.A., Leonard, S.J., Hardyman, M.A., Vaniotis, G., Allen, B.G. et al. (2015) Cardiac protein kinases: the cardiomyocyte kinome and differential kinase expression in human failing hearts. *Cardiovasc. Res.* **108**, 87–98, https://doi.org/10.1093/cvr/cvv210
19 Muslin, A.J. (2005) Role of raf proteins in cardiac hypertrophy and cardiomyocyte survival. *Trends Cardiovasc. Med.* **15**, 225–229, https://doi.org/10.1016/j.tcm.2005.06.008
20 Meijles, D.N., Cull, J.J., Cooper, S.T.E., Markou, T., Hardyman, M.A., Fuller, S.J. et al. (2021) The anti-cancer drug dabrafenib is not cardiotoxic and inhibits cardiac remodelling and fibrosis in a murine model of hypertension. *Clin. Sci. (Lond.)* **135**, 1631–1647, https://doi.org/10.1042/CS20210192
21 Marshall, J.J.T., Cull, J.J., Alharbi, H.O., Zaw Thin, M., Cooper, S.T.E., Barrington, C. et al. (2022) PKN2 deficiency leads both to prenatal 'congenital' cardiomyopathy and defective angiotensin II stress responses. *Biochem. J.* **479**, 1467–1486, https://doi.org/10.1042/BCJ20220281
22 Chen, A.P., Ohno, M., Giese, K.P., Kühn, R., Chen, R.L. and Silva, A.J. (2006) Forebrain-specific knockout of B-raf kinase leads to deficits in hippocampal long-term potentiation, learning, and memory. *J. Neurosci. Res.* **83**, 28–38, https://doi.org/10.1002/jnr.20703
23 Sohal, D.S., Nghiem, M., Crackower, M.A., Witt, S.A., Kimball, T.R., Tymitz, K.M. et al. (2001) Temporally regulated and tissue-specific gene manipulations in the adult and embryonic heart using a tamoxifen-inducible Cre protein. *Circ. Res.* **89**, 20–25, https://doi.org/10.1161/hh1301.092687
24 Meijles, D.N., Cull, J.J., Markou, T., Cooper, S.T.E., Haines, Z.H.R., Fuller, S.J. et al. (2020) Redox regulation of cardiac ASK1 (Apoptosis Signal-Regulating Kinase 1) controls p38-MAPK (mitogen-activated protein kinase) and orchestrates cardiac remodeling to hypertension. *Hypertension* **76**, 1208–1218, https://doi.org/10.1161/HYPERTENSIONAHA.119.14556
25 Patel, J., Douglas, G., Kerr, A.G., Hale, A.B. and Channon, K.M. (2018) Effect of irradiation and bone marrow transplantation on angiotensin II-induced aortic inflammation in ApoE knockout mice. *Atherosclerosis* **276**, 74–82, https://doi.org/10.1016/j.atherosclerosis.2018.07.019
26 Capone, C., Faraco, G., Peterson, J.R., Coleman, C., Anrather, J., Milner, T.A. et al. (2012) Central cardiovascular circuits contribute to the neurovascular dysfunction in angiotensin II hypertension. *J. Neurosci.* **32**, 4878–4886, https://doi.org/10.1523/JNEUROSCI.6262-11.2012

27 Zimmerman, M.C., Lazartigues, E., Sharma, R.V. and Davisson, R.L. (2004) Hypertension caused by angiotensin II infusion involves increased superoxide production in the central nervous system. *Circ. Res.* **95**, 210–216, https://doi.org/10.1161/01.RES.0000135483.12297.e4
28 Izumiya, Y., Kim, S., Izumi, Y., Yoshida, K., Yoshiyama, M., Matsuzawa, A. et al. (2003) Apoptosis signal-regulating kinase 1 plays a pivotal role in angiotensin II-induced cardiac hypertrophy and remodeling. *Circ. Res.* **93**, 874–883, https://doi.org/10.1161/01.RES.0000100665.67510.F5
29 Meijles, D.N., Fuller, S.J., Cull, J.J., Alharbi, H.O., Cooper, S.T.E., Sugden, P.H. et al. (2021) The insulin receptor family and protein kinase B (Akt) are activated in the heart by alkaline pH and alpha1-adrenergic receptors. *Biochem. J.* **478**, 2059–2079, https://doi.org/10.1042/BCJ20210144
30 Iulita, M.F., Vallerand, D., Beauvillier, M., Haupert, N., Ulysse, C.A., Gagne, A. et al. (2018) Differential effect of angiotensin II and blood pressure on hippocampal inflammation in mice. *J. Neuroinflammation* **15**, 62, https://doi.org/10.1186/s12974-018-1090-z
31 Marshall, A.K., Barrett, O.P.T., Cullingford, T.E., Shanmugasundram, A., Sugden, P.H. and Clerk, A. (2010) ERK1/2 signaling dominates over RhoA signaling in regulating early changes in RNA expression induced by endothelin-1 in neonatal rat cardiomyocytes. *PLoS ONE* **5**, e10027, https://doi.org/10.1371/journal.pone.0010027
32 Jahn, H.M., Kasakow, C.V., Helfer, A., Michely, J., Verkhratsky, A., Maurer, H.H. et al. (2018) Refined protocols of tamoxifen injection for inducible DNA recombination in mouse astroglia. *Sci. Rep.* **8**, 5913, https://doi.org/10.1038/s41598-018-24085-9
33 Hougen, K., Aronsen, J.M., Stokke, M.K., Enger, U., Nygard, S., Andersson, K.B. et al. (2010) Cre-loxP DNA recombination is possible with only minimal unspecific transcriptional changes and without cardiomyopathy in Tg(αMHC-MerCreMer) mice. *Am. J. Physiol. Heart Circ. Physiol.* **299**, H1671–H1678, https://doi.org/10.1152/ajpheart.01155.2009
34 Zhou, P. and Pu, W.T. (2016) Recounting cardiac cellular composition. *Circ. Res.* **118**, 368–370, https://doi.org/10.1161/CIRCRESAHA.116.308139
35 Paradis, A.N., Gay, M.S. and Zhang, L. (2014) Binucleation of cardiomyocytes: the transition from a proliferative to a terminally differentiated state. *Drug Discov. Today* **19**, 602–609, https://doi.org/10.1016/j.drudis.2013.10.019
36 Peyronnet, R., Nerbonne, J.M. and Kohl, P. (2016) Cardiac mechano-gated ion channels and arrhythmias. *Circ. Res.* **118**, 311–329, https://doi.org/10.1161/CIRCRESAHA.115.305043
37 Lyon, R.C., Zanella, F., Omens, J.H. and Sheikh, F. (2015) Mechanotransduction in cardiac hypertrophy and failure. *Circ. Res.* **116**, 1462–1476, https://doi.org/10.1161/CIRCRESAHA.116.304937
38 Marasciulo, F.L., Montagnani, M. and Potenza, M.A. (2006) Endothelin-1: the yin and yang on vascular function. *Curr. Med. Chem.* **13**, 1655–1665, https://doi.org/10.2174/092986706777441968
39 Frangogiannis, N.G. (2019) Cardiac fibrosis: Cell biological mechanisms, molecular pathways and therapeutic opportunities. *Mol. Aspects Med.* **65**, 70–99, https://doi.org/10.1016/j.mam.2018.07.001
40 Corden, B., Adami, E., Sweeney, M., Schafer, S. and Cook, S.A. (2020) IL-11 in cardiac and renal fibrosis: Late to the party but a central player. *Br. J. Pharmacol.* **177**, 1695–1708, https://doi.org/10.1111/bph.15013
41 Sweeney, M., Corden, B. and Cook, S.A. (2020) Targeting cardiac fibrosis in heart failure with preserved ejection fraction: mirage or miracle? *EMBO Mol. Med.* **12**, e10865, https://doi.org/10.15252/emmm.201910865
42 Nicin, L., Wagner, J.U.G., Luxán, G. and Dimmeler, S. (2022) Fibroblast-mediated intercellular crosstalk in the healthy and diseased heart. *FEBS Lett.* **596**, 638–654, https://doi.org/10.1002/1873-3468.14234
43 Zhang, M., Perino, A., Ghigo, A., Hirsch, E. and Shah, A.M. (2013) NADPH oxidases in heart failure: poachers or gamekeepers? *Antioxid Redox Signal.* **18**, 1024–1041, https://doi.org/10.1089/ars.2012.4550
44 O'Connell, T.D., Jensen, B.C., Baker, A.J. and Simpson, P.C. (2014) Cardiac alpha$_1$-adrenergic receptors: novel aspects of expression, signaling mechanisms, physiologic function, and clinical importance. *Pharmacol. Rev.* **66**, 308–333, https://doi.org/10.1124/pr.112.007203
45 Foryst-Ludwig, A. and Kintscher, U. (2013) Sex differences in exercise-induced cardiac hypertrophy. *Pflugers Arch.* **465**, 731–737, https://doi.org/10.1007/s00424-013-1225-0
46 Gibb, A.A. and Hill, B.G. (2018) Metabolic coordination of physiological and pathological cardiac remodeling. *Circ. Res.* **123**, 107–128, https://doi.org/10.1161/CIRCRESAHA.118.312017
47 Singh, R.B., Sozzi, F.B., Fedacko, J., Hristova, K., Fatima, G., Pella, D. et al. (2022) Pre-heart failure at 2D- and 3D-speckle tracking echocardiography: a comprehensive review. *Echocardiography* **39**, 302–309, https://doi.org/10.1111/echo.15284
48 Szokodi, I., Kerkela, R., Kubin, A.M., Sarman, B., Pikkarainen, S., Konyi, A. et al. (2008) Functionally opposing roles of extracellular signal-regulated kinase 1/2 and p38 mitogen-activated protein kinase in the regulation of cardiac contractility. *Circulation* **118**, 1651–1658, https://doi.org/10.1161/CIRCULATIONAHA.107.758623
49 Fliegel, L. (2019) Structural and functional changes in the Na(+)/H(+) Exchanger Isoform 1, Induced by Erk1/2 phosphorylation. *Int. J. Mol. Sci.* **20**, 2378, https://doi.org/10.3390/ijms20102378
50 Mraiche, F., Oka, T., Gan, X.T., Karmazyn, M. and Fliegel, L. (2011) Activated NHE1 is required to induce early cardiac hypertrophy in mice. *Basic Res. Cardiol.* **106**, 603–616, https://doi.org/10.1007/s00395-011-0161-4
51 Chen, J., Fujii, K., Zhang, L., Roberts, T. and Fu, H. (2001) Raf-1 promotes cell survival by antagonizing apoptosis signal-regulating kinase 1 through a MEK-ERK independent mechanism. *Proc. Natl. Acad. Sci. U.S.A.* **98**, 7783–7788, https://doi.org/10.1073/pnas.141224398
52 O'Neill, E., Rushworth, L., Baccarini, M. and Kolch, W. (2004) Role of the kinase MST2 in suppression of apoptosis by the proto-oncogene product Raf-1. *Science* **306**, 2267–2270, https://doi.org/10.1126/science.1103233
53 Camper-Kirby, D., Welch, S., Walker, A., Shiraishi, I., Setchell, K.D.R., Schaefer, E. et al. (2001) Myocardial Akt activation and gender: increased nuclear activity in females versus males. *Circ. Res.* **88**, 1020–1027, https://doi.org/10.1161/hh1001.090858
54 Sugden, P.H. and Clerk, A. (2001) Akt like a woman: gender differences in susceptibility to cardiovascular disease. *Circ. Res.* **88**, 975–977, https://doi.org/10.1161/hh1001.091864
55 Pinzi, L. (2022) On the development of B-Raf inhibitors acting through innovative mechanisms. *F1000Res.* **11**, 237, https://doi.org/10.12688/f1000research.108761.2

SUPPLEMENTARY DATA

Cardiomyocyte BRAF is a key signalling intermediate in cardiac hypertrophy in mice.

Hajed O. Alharbi[1], Michelle A. Hardyman[1], Joshua J. Cull[1], Thomais Markou[1], Susanna T.E. Cooper[2], Peter E. Glennon[3], Stephen J. Fuller[1], Peter H. Sugden[1] and Angela Clerk[1]

[1] School of Biological Sciences, University of Reading, Reading, UK

[2] Molecular and Clinical Sciences Institute, St. George's University of London, London, UK.

[3] University Hospitals Coventry and Warwickshire, University Hospital Cardiology Department, Clifford Bridge Road, Coventry, UK.

Supplementary Figure S1. Ratios of heart weight (HW) to body weight (BW). Male (**A**) or female (**B**) $BRAF^{fl/fl}/Cre^{+/-}$ mice were treated with corn-oil (CO) or tamoxifen in corn-oil (Tx) 4 days before minipumps were implanted for delivery of PBS or acidified PBS (Vehicle) or 0.8 mg/kg/d angiotensin II in AcPBS (AngII), or 40 mg/kg/d phenylephrine (PE) for 7 d. Heart and body weights were taken at the end of the experiment.

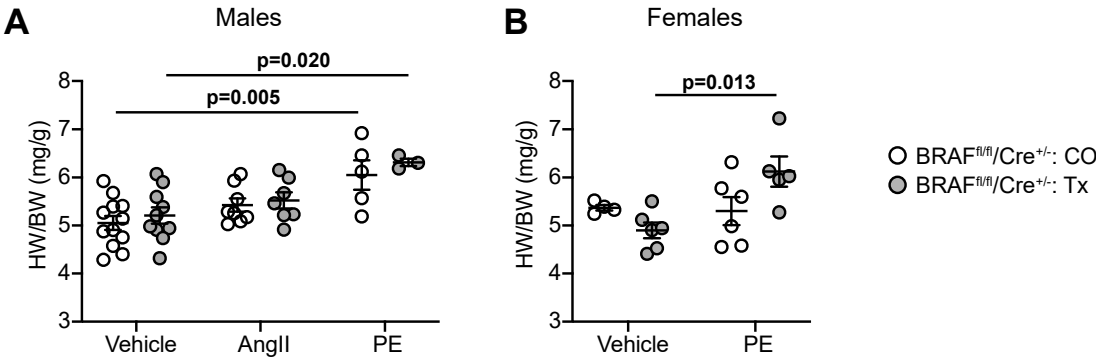

Supplementary Table S1. Mouse weights (g). Mice were allocated to groups on a random basis and were treated with corn-oil (CO) or tamoxifen in corn-oil (Tx) with acidified PBS (AcPBS) or 0.8 mg/kg/d angiotensin II (AngII), or with PBS or 40 mg/kg/d phenylephrine in PBS (PE). Weights were taken at the start of the study with the first baseline echocardiogram (Start), immediately after minipump surgery, and when mice were culled (End). Weights post-surgery and at the end included the minipumps. Male mice were 7-8 weeks at the start of the experiment; female mice were 9-10 weeks at the start of the experiment.

Study	**Condition**	**Start**		**Post-minipump**		**End**		
		Mean	**SEM**	**Mean**	**SEM**	**Mean**	**SEM**	**n**
$Cre^{+/-}$								
AngII (males)	CO/AcPBS	22.45	1.07	24.60	0.55	25.28	0.68	4
(echocardiography	Tx/AcPBS	22.14	1.18	23.80	1.36	24.08	1.37	5
+ biochemistry)	CO/AngII	22.28	1.21	23.35	0.95	23.95	0.79	6
	Tx/AngII	22.82	1.07	23.92	0.82	24.08	0.77	5
$BRAF^{fl/fl}/Cre^{+/-}$								
AngII (males)	CO/AcPBS	24.01	0.56	25.01	0.48	25.10	0.44	10
(echocardiography	Tx/AcPBS	24.70	0.48	25.93	0.44	26.13	0.40	8
+ biochemistry)	CO/AngII	25.17	0.38	26.60	0.33	26.12	0.64	10
	Tx/AngII	23.83	0.54	25.10	0.45	24.93	0.37	10
AngII (males)	CO/AcPBS	23.65	0.54	26.36	0.49	26.96	0.57	8
(histology)	Tx/AcPBS	22.33	0.31	25.23	0.30	26.05	0.17	4
	CO/AngII	24.29	0.28	26.60	0.26	26.80	0.37	7
	Tx/AngII	22.88	0.70	26.30	0.56	26.36	0.58	5
PE (males)	CO/PBS	23.77	0.55	25.07	0.36	25.54	0.39	7
	Tx/PBS	23.55	0.41	25.49	0.38	25.71	0.43	8
	CO/PE	23.89	0.75	25.13	0.63	24.73	0.61	8
	Tx/PE	23.06	0.75	24.29	0.53	24.51	0.44	8
PE (females)	CO/PBS	19.64	0.52	21.10	0.58	21.31	0.58	9
	Tx/PBS	19.19	0.39	20.96	0.28	20.99	0.21	10
	CO/PE	19.19	0.58	20.20	0.49	20.47	0.43	10
	Tx/PE	19.64	0.60	20.77	0.40	20.74	0.35	10

Supplementary Table S2. Primers for genotyping and confirmation of recombination.

Mouse strain	DNA	Forward primer	Reverse primer	Annealing temp.
Genotyping				
$BRAF^{fl/fl}$	gDNA	GCATAGCGCATATGCTCACA	CCATGCTCTAACTAGTGCTG	57°C
Cre^{-}	gDNA	TCTATTGCACACAGCAATCCA	CCAACTCTTGTGAGAGGAGCA	52°C
Cre^{+}	gDNA	TCTATTGCACACAGCAATCCA	CCAGCATTGTGAGAACAAGG	52°C
Recombination				
$BRAF^{fl/fl}$ (exons 9-13)	cDNA	TTGATTTTGAGCCTGGCCCAGTG	GTGCAGTCTGCCGAGCAATATC	57°C
$BRAF^{fl/fl}$ (exons 10-13)	cDNA	GTCATCTTCTTCCTCATCCTCG	GTGCAGTCTGCCGAGCAATATC	57°C

Supplementary S3. qPCR primers.

Gene Symbol	Accession No.	Sense Primer (5'→3')	Antisense Primer (5'→3')
Col1a1	NM_007742	TCGTGGCTTCTCTGGTCTC	CCGTTGAGTCCGTCTTTGC
Col4a1	NM_009931.2	TGTGGGCCAGCCAGGCATTG	CAGGGGGTCCGATCGCTCCA
Ctgf	NM_010217	GCACACCGCACAGAACCA	ATGGCAGGCACAGGTCTTG
Ddr2	NM_022563.2	GCACTTGGTGAATTAATTAGAATCCTG	GGACAACTAAATGGTCCCTCCC
Edn1	NM_007913	GCCTTCGCTCACTCCACTA	GCTGGGATTGGTAGGTGGTA
Fn1	NM_010233	AAGAGGACGTTGCAGAGCTA	AGACACTGGAGACACTGACTAA
Gapdh	NM_008084.2	TCACCACCATGGAGAAGGC	GCTAAGCAGTTGGTGGTGCA
Hif1a	NM_010431	GATGTAATGTTTCCCTCTTCTAATGA	GCAGGATCAGCACTACTTCG
Il6	NM_031168	TCCATCCAGTTGCCTTCTTG	GGTCTGTTGGGAGTGGTATC
Il1b	NM_008361	CAACCAACAAGTGATATTCTCCAT	GGGTGTGCCGTCTTTCATTA
Lox	NM_001286181	GACATTCGCTACACAGGACAT	AACACCAGGTACGGCTTTATC
Myh6	NM_010856	CGAGCTGGATGAGGCGGAG	TCTGCTGGAGAGGTTATTCCTCG
Myh7	NM_080728	CATGCCAACCGTATGGCTG	GTTCCACGATGGCGATGTTC
Nppa	NM_008725	GATGGATTTCAAGAACCTGCTAGA	CTTCCTCAGTCTGCTCACTCA
Nppb	NM_008726	TCCAGCAGAGACCTCAAAATTC	CAGTGCGTTACAGCCCAAA
Postn	NM_015784	TTCCTCTCCTGCCCTTATATGC	CCTGATCCCGACCCCTGAT
NOX1	NM_172203	CATCCCTTCACTCTGACTTCTG	GCAGGTGCTAGCTTACAAATG GTCCTTATG
NOX2 (Cybb)	NM_007807	GCTATGAGGTGGTGATGTTAGT	GTTTCAGACTGGTGGCATTATC
NOX4	NM_015760	GGAAGCCCATTTGAGGAGTC	TCCAGTCATCCAGTAGAGTGTT
Tgfb1	NM_011577	TGGACACACAGTACAGCAAG	GTAGTAGACGATGGGCAGTG

Supplementary Table S4. Echocardiography data for hemizygous Cre$^{+/-}$ male mice treated without/with angiotensin II. Male Cre$^{+/-}$ mice (7-8 weeks) were treated with corn-oil (CO) or tamoxifen in corn-oil (Tx) 4 days before minipumps were implanted for delivery of acidified PBS (AcPBS) or 0.8 mg/kg/d angiotensin II in AcPBS (AngII) for 7 d. Echocardiograms were taken prior to tamoxifen treatment (Baseline) and 7 d after minipump implantation. Echocardiograms were analysed using VevoLab software. LV, left ventricle; ID, internal diameter; AW, anterior wall; PW, posterior wall; WT, wall thickness (AW+PW); EDV, end diastolic volume; ESV, end systolic volume; EDLVM, end diastolic LV mass; ESLVM, end systolic LV mass.

* Data collected from B-mode images of long axis views. Other parameters were measured from M-mode images of short axis views.

7 d	**CO/AcPBS (n=4)**		**Tx/AcPBS (n=5)**		**CO/AngII (n=6)**		**Tx/AngII (n=5)**	
	Mean	SEM	Mean	SEM	Mean	SEM	Mean	SEM
Heart Rate (bpm)	470	24	446	9	471	21	479	17
LVID;s (mm)	3.380	0.113	3.254	0.125	2.962	0.213	2.746	0.114
LVID;d (mm)	4.356	0.131	4.215	0.192	3.873	0.150	3.757	0.177
LVAW;s (mm)	0.887	0.050	0.958	0.023	0.993	0.040	1.091	0.041
LVAW;d (mm)	0.736	0.029	0.747	0.006	0.785	0.022	0.866	0.027
LVPW;s (mm)	0.931	0.059	0.939	0.064	1.096	0.064	1.096	0.041
LVPW;d (mm)	0.698	0.039	0.722	0.032	0.855	0.069	0.829	0.077
EDV (µl)*	59.40	4.98	59.46	8.36	46.83	4.16	46.53	5.32
ESV (µl)*	32.26	2.96	29.47	2.90	24.92	2.16	21.44	2.17
EDLVM (mg)*	59.81	1.42	57.65	2.40	70.02	1.88	66.48	1.15
ESLVM (mg)*	62.78	1.19	61.35	3.75	71.50	2.01	70.50	0.86
Stroke Volume (µl)*	27.14	2.29	29.99	6.04	21.91	2.62	25.09	3.15
Ejection Fraction (%)*	45.65	1.41	49.09	3.20	46.35	2.54	53.26	0.68
Fractional Shortening (%)*	22.16	2.20	24.68	2.32	23.94	1.15	26.02	3.11
Cardiac Output (ml/min)*	12.37	0.88	12.85	2.73	9.78	1.17	10.92	1.07
GLS (%)*	-16.60	2.17	-15.87	0.62	-14.88	1.61	-17.53	1.28
GCS (%)*	-17.30	1.23	-18.98	1.48	-18.87	1.14	-20.93	1.36

Supplementary Table S5. Echocardiography data for male mice with cardiomyocyte BRAF knockout treated without/with angiotensin II. Male $BRAF^{fl/fl}/Cre^{+/-}$ mice (7-8 weeks) were treated with corn-oil (CO) or tamoxifen in corn-oil (Tx) 4 days before minipumps were implanted for delivery of acidified PBS (AcPBS) or 0.8 mg/kg/d angiotensin II in AcPBS (AngII) for 7 d. Echocardiograms were taken prior to tamoxifen treatment (Baseline) and 7 d after minipump implantation. Echocardiograms were analysed using VevoLab software. LV, left ventricle; ID, internal diameter; AW, anterior wall; PW, posterior wall; WT, wall thickness (AW+PW); EDV, end diastolic volume; ESV, end systolic volume; EDLVM, end diastolic LV mass; ESLVM, end systolic LV mass.

* Data collected from B-mode images of long axis views. Other parameters were measured from M-mode images of short axis views.

Baseline	**CO/AcPBS (n=10)**		**Tx/AcPBS (n=8)**		**CO/AngII (n=10)**		**Tx/AngII (n=10)**	
	Mean	SEM	Mean	SEM	Mean	SEM	Mean	SEM
Heart Rate (bpm)	463	17	476	10	463	10	462	10
LVID;s (mm)	2.929	0.163	3.020	0.093	3.016	0.128	3.165	0.043
LVID;d (mm)	3.984	0.110	3.978	0.076	3.985	0.097	4.157	0.031
LVAW;s (mm)	0.981	0.024	0.943	0.018	0.935	0.016	0.949	0.013
LVAW;d (mm)	0.728	0.015	0.717	0.011	0.726	0.015	0.738	0.012
LVPW;s (mm)	0.967	0.036	0.909	0.032	0.939	0.016	0.941	0.028
LVPW;d (mm)	0.685	0.020	0.670	0.019	0.691	0.014	0.670	0.018
EDV (µl)*	51.36	2.91	52.97	1.85	49.45	2.35	47.74	1.56
ESV (µl)*	26.95	2.24	28.21	1.53	27.99	2.20	25.19	1.30
EDLVM (mg)*	55.87	2.19	53.42	1.77	56.67	2.28	52.32	1.96
ESLVM (mg)*	58.39	2.02	56.68	1.75	58.87	2.11	55.19	1.96
Stroke Volume (µl)	35.46	1.56	33.31	1.19	33.52	0.96	36.74	1.05
Ejection Fraction (%)	52.30	3.72	48.47	1.88	49.01	2.51	47.92	1.31
Fractional Shortening (%)	27.04	2.54	24.21	1.12	24.61	1.56	23.88	0.79
Cardiac Output (ml/min)	16.26	0.64	15.85	0.68	15.46	0.51	16.95	0.57
7 d	**CO/AcPBS (n=10)**		**Tx/AcPBS (n=8)**		**CO/AngII (n=10)**		**Tx/AngII (n=10)**	
	Mean	SEM	Mean	SEM	Mean	SEM	Mean	SEM
Heart Rate (bpm)	488	20	500	9	512	15	489	21
LVID;s (mm)	3.000	0.118	2.986	0.128	2.515	0.147	2.651	0.189
LVID;d (mm)	3.998	0.087	4.024	0.104	3.581	0.125	3.771	0.133
LVAW;s (mm)	0.976	0.026	0.980	0.034	1.160	0.043	1.122	0.081
LVAW;d (mm)	0.751	0.020	0.715	0.015	0.907	0.030	0.867	0.043
LVPW;s (mm)	0.963	0.043	0.942	0.019	1.217	0.049	1.157	0.060
LVPW;d (mm)	0.699	0.031	0.662	0.018	0.899	0.032	0.815	0.049
EDV (µl)*	47.14	2.80	51.97	3.36	39.36	2.50	37.87	3.43
ESV (µl)*	28.22	2.43	27.17	2.03	20.96	1.74	19.66	2.72
EDLVM (mg)*	52.97	1.41	55.25	1.72	69.40	2.53	64.24	4.73
ESLVM (mg)*	55.55	1.77	59.09	1.71	72.32	2.60	67.32	5.07
Stroke Volume (µl)	34.43	2.01	36.09	1.85	30.63	1.78	33.95	1.90
Ejection Fraction (%)	49.69	3.07	51.21	2.67	57.88	3.07	57.26	4.29
Fractional Shortening (%)	25.18	1.93	26.00	1.69	30.46	2.28	30.42	3.09

Supplementary Table S6. Echocardiography data for male mice with cardiomyocyte BRAF knockout treated without/with phenylephrine. Male $BRAF^{fl/fl}/Cre^{+/-}$ mice (7-8 weeks) were treated with corn-oil (CO) or tamoxifen in corn-oil (Tx) 4 days before minipumps were implanted for delivery of PBS or 40 mg/kg/d phenylephrine in PBS (PE) for 7 d. Echocardiograms were taken prior to tamoxifen treatment (Baseline) and 7 d after minipump implantation. Echocardiograms were analysed. LV, left ventricle; ID, internal diameter; AW, anterior wall; PW, posterior wall; WT, wall thickness (AW+PW); EDV, end diastolic volume; ESV, end systolic volume; EDLVM, end diastolic LV mass; ESLVM, end systolic LV mass; GLS, global longitudinal strain; GCS, global circumferential strain.

* Data collected from B-mode images were analysed using VevoStrain software. Other parameters were measured from M-mode images of short axis views using VevoLab software.

Baseline	**CO/PBS (n=7)**		**Tx/PBS (n=8)**		**CO/PE (n=8)**		**Tx/PE (n=8)**	
	Mean	SEM	Mean	SEM	Mean	SEM	Mean	SEM
Heart Rate (bpm)	457	10	469	12	459	12	474	15
LVID;s (mm)	2.697	0.125	2.421	0.113	2.723	0.096	2.315	0.127
LVID;d (mm)	3.908	0.126	3.729	0.102	3.920	0.091	3.653	0.088
LVAW;s (mm)	1.014	0.016	1.025	0.018	1.012	0.024	1.054	0.030
LVAW;d (mm)	0.744	0.012	0.760	0.007	0.752	0.012	0.773	0.012
LVPW;s (mm)	1.003	0.018	1.093	0.037	1.011	0.030	1.058	0.037
LVPW;d (mm)	0.686	0.024	0.711	0.015	0.701	0.019	0.704	0.020
EDV (µl)*	46.42	4.29	42.65	2.43	46.10	1.52	40.69	3.20
ESV (µl)*	19.01	1.75	16.72	1.88	20.49	1.51	15.52	2.62
EDLVM (mg)*	50.25	2.32	49.31	1.12	49.51	1.80	49.24	1.99
ESLVM (mg)*	51.80	2.52	50.72	1.27	50.67	1.79	50.09	2.30
Stroke Volume (µl)*	27.41	2.77	25.94	1.31	25.61	1.40	25.17	1.47
Ejection Fraction (%)*	59.43	1.75	61.25	3.04	55.27	2.64	63.52	4.28
Fractional Shortening (%)*	31.23	1.70	34.86	2.59	28.28	2.97	36.95	3.67
Cardiac Output (ml/min)*	12.30	1.26	12.13	0.70	11.46	0.83	11.67	0.57
GLS (%)*	-20.62	1.02	-21.27	1.02	-19.03	0.88	-20.52	1.72
GCS (%)*	-21.43	1.69	-24.66	1.48	-21.89	1.24	-25.33	1.66
7 d	**CO/PBS (n=7)**		**Tx/PBS (n=8)**		**CO/PE (n=8)**		**Tx/PE (n=8)**	
	Mean	SEM	Mean	SEM	Mean	SEM	Mean	SEM
Heart Rate (bpm)	485	18	513	9	470	15	465	17
LVID;s (mm)	2.622	0.130	2.636	0.118	2.137	0.151	1.920	0.126
LVID;d (mm)	3.841	0.119	3.917	0.105	3.505	0.121	3.307	0.077
LVAW;s (mm)	1.041	0.028	1.101	0.031	1.276	0.064	1.297	0.076
LVAW;d (mm)	0.771	0.012	0.801	0.017	0.865	0.038	0.917	0.054
LVPW;s (mm)	1.029	0.028	1.072	0.032	1.301	0.095	1.405	0.099
LVPW;d (mm)	0.697	0.027	0.708	0.024	0.974	0.089	1.000	0.094
EDV (µl)*	47.61	3.65	48.06	3.10	34.69	3.07	32.84	2.94
ESV (µl)*	18.74	1.97	19.72	2.10	10.64	1.45	9.91	1.47
EDLVM (mg)*	53.23	2.60	51.93	1.41	68.34	3.36	67.43	4.89
ESLVM (mg)*	55.29	2.98	53.82	1.50	70.73	3.65	69.15	5.33
Stroke Volume (µl)*	28.87	2.58	28.33	1.50	24.04	1.83	22.93	1.83
Ejection Fraction (%)*	60.44	2.76	59.13	2.42	70.04	1.95	70.30	2.48
Fractional Shortening (%)*	32.02	3.56	32.85	2.40	40.67	2.84	41.67	1.90
Cardiac Output (ml/min)*	13.67	0.87	13.83	0.92	11.29	0.92	10.65	1.00
GLS (%)*	-19.70	1.55	-20.90	1.18	-23.33	1.05	-19.44	1.44
GCS (%)*	-22.79	1.69	-23.22	0.75	-28.33	1.33	-28.57	2.05

Supplementary Table S7. Echocardiography data for female mice with cardiomyocyte BRAF knockout treated without/with phenylephrine. Female $BRAF^{fl/fl}/Cre^{+/-}$ mice (9-10 weeks) were treated with corn-oil (CO) or tamoxifen in corn-oil (Tx) 4 days before minipumps were implanted for delivery of PBS or 40 mg/kg/d phenylephrine in PBS (PE) for 7 d. Echocardiograms were taken prior to tamoxifen treatment (Baseline) and 7 d after minipump implantation. Echocardiograms were analysed. LV, left ventricle; ID, internal diameter; AW, anterior wall; PW, posterior wall; WT, wall thickness (AW+PW); EDV, end diastolic volume; ESV, end systolic volume; EDLVM, end diastolic LV mass; ESLVM, end systolic LV mass; GLS, global longitudinal strain; GCS, global circumferential strain.

* Data collected from B-mode images were analysed using VevoStrain software. Other parameters were measured from M-mode images of short axis views using VevoLab software.

Baseline	**CO/PBS (n=9)**		**Tx/PBS (n=10)**		**CO/PE (n=10)**		**Tx/PE (n=10)**	
	Mean	SEM	Mean	SEM	Mean	SEM	Mean	SEM
Heart Rate (bpm)	457	17	464	7	465	14	452	10
LVID;s (mm)	2.576	0.104	2.556	0.061	2.569	0.113	2.636	0.089
LVID;d (mm)	3.726	0.067	3.632	0.055	3.671	0.113	3.743	0.069
LVAW;s (mm)	0.941	0.008	0.948	0.011	0.959	0.021	0.917	0.014
LVAW;d (mm)	0.713	0.008	0.716	0.008	0.696	0.015	0.700	0.009
LVPW;s (mm)	0.938	0.026	0.917	0.012	0.907	0.018	0.933	0.018
LVPW;d (mm)	0.639	0.011	0.657	0.018	0.650	0.021	0.650	0.011
EDV (µl)*	38.34	2.64	40.18	1.15	39.53	2.96	41.20	2.10
ESV (µl)*	15.70	2.42	17.31	1.24	17.42	2.07	18.52	1.57
EDLVM (mg)*	43.46	1.48	43.45	1.21	43.65	1.99	43.69	1.57
ESLVM (mg)*	44.50	1.53	44.70	1.61	45.34	2.14	44.76	1.66
Stroke Volume (µl)*	22.64	0.99	22.87	1.01	22.11	1.08	22.68	0.72
Ejection Fraction (%)*	60.72	3.79	57.11	2.54	56.94	2.25	55.50	1.68
Fractional Shortening (%)*	33.71	2.86	31.65	2.09	31.15	2.09	30.91	1.62
Cardiac Output (ml/min)*	10.34	0.50	10.49	0.56	10.11	0.62	9.93	0.34
GLS (%)*	-21.15	1.69	-19.50	1.33	-18.41	0.78	-18.69	0.76
GCS (%)*	-21.76	1.54	-22.21	1.36	-22.76	1.23	-20.35	0.96
7 d	**CO/PBS (n=9)**		**Tx/PBS (n=10)**		**CO/PE (n=10)**		**Tx/PE (n=10)**	
	Mean	SEM	Mean	SEM	Mean	SEM	Mean	SEM
Heart Rate (bpm)	487	16	478	13	471	13	447	11
LVID;s (mm)	2.570	0.142	2.508	0.093	1.995	0.118	1.946	0.109
LVID;d (mm)	3.786	0.106	3.632	0.045	3.310	0.090	3.293	0.098
LVAW;s (mm)	1.004	0.025	1.001	0.017	1.183	0.058	1.261	0.086
LVAW;d (mm)	0.739	0.021	0.726	0.010	0.821	0.031	0.900	0.052
LVPW;s (mm)	1.004	0.045	0.958	0.021	1.249	0.076	1.282	0.096
LVPW;d (mm)	0.674	0.014	0.677	0.022	0.883	0.076	0.919	0.090
EDV (µl)*	36.36	2.52	38.51	1.78	30.70	2.06	31.39	2.33
ESV (µl)*	15.89	2.34	15.81	1.40	11.57	1.00	9.42	0.73
EDLVM (mg)*	49.56	2.09	51.12	1.66	57.60	5.03	63.09	5.35
ESLVM (mg)*	51.19	2.05	52.90	1.90	59.42	5.29	64.74	5.32
Stroke Volume (µl)*	20.47	1.37	22.71	1.02	19.13	1.49	21.97	1.85
Ejection Fraction (%)*	57.50	4.36	59.04	2.27	61.68	2.44	69.25	1.90
Fractional Shortening (%)*	30.83	3.50	32.53	1.88	33.77	2.45	43.86	2.60
Cardiac Output (ml/min)*	9.91	0.85	11.01	0.67	8.64	0.69	9.65	1.03
GLS (%)*	-18.45	1.86	-19.59	0.72	-19.67	1.55	-20.51	1.55
GCS (%)*	-23.21	1.78	-21.77	1.53	-26.72	1.78	-28.36	1.77